https://doi.org/10.5194/wes-2025-265
Preprint. Discussion started: 8 December 2025

eawe european academy of wind energy
Open Access WIND ENERGY SCIENCE DISCUSSIONS

Combining wake steering and active wake mixing on a large-scale wind farm

Matteo Baricchio[1], Daan van der Hoek[1], Tim Dammann[1], Pieter M. O. Gebraad[2], Jenna Iori[3], and Jan-Willem van Wingerden[1]

[1]Faculty of Mechanical Engineering, Delft University of Technology, Delft, the Netherlands
[2]Youwind, Barcelona, Spain
[3]Faculty of Aerospace Engineering, Delft University of Technology, Delft, the Netherlands

Correspondence: Matteo Baricchio (m.baricchio@tudelft.nl)

Abstract. Wind farm flow control mitigates wake effects within a wind farm by adjusting the turbine settings to improve the overall farm performance rather the output of each turbine. Wake steering is an established approach while active wake mixing has recently emerged as a promising solution. This study quantifies the value of a combined strategy, in which each turbine can apply wake steering or the helix. The analysis is performed considering different degrees of uncertainty in wind direction using engineering wake models which enable the simulation of these techniques on large-scale wind farms. A novel optimization algorithm, called Multi-strategy Serial-Refine (MSR), is developed in this study, extending the state-of-the-art method for yaw optimization to multiple control strategies and a generalized objective. A scaled version of an offshore wind farm in the Netherlands is selected as the case study, consisting of 69 IEA 22 MW turbines. The proposed combined strategy yields a 1.98 % increase in annual energy production compared to the baseline scenario, in contrast to the 1.68 % and 1.15 % gains obtained by applying only wake steering or the helix, respectively. This trend persists under wind direction uncertainty. Given the pronounced sensitivity of wake steering to such uncertainty, the combined strategy takes advantage of the superior robustness of the helix under these circumstances.

1 Introduction

Wind farm flow control (WFFC) provides a valid and promising solution to mitigate wake losses within a wind farm and enhance power production (Meyers et al., 2022). It consists of optimizing the performance of the entire farm collectively, in contrast to a greedy operation where the power production of the turbines is maximized individually (van Wingerden et al., 2020). In recent years, different WFFC techniques have been developed. These can be divided into two main categories, namely quasi-static and dynamic WFFC (Meyers et al., 2022), where the latter are often referred to as active wake mixing techniques.

Among the quasi-static strategies, wake steering has emerged as one of the most effective solutions (Doekemeijer et al., 2021). It consists of diverting the wakes from the downstream rotors by intentionally misaligning the turbines with the wind direction, hence using the yaw angle as control variable. The efficacy of this technique has been widely demonstrated through large eddy simulations (LES), wind tunnel tests and field experiments (Fleming et al., 2014; Gebraad et al., 2016; Campagnolo et al., 2020; Doekemeijer et al., 2021).

https://doi.org/10.5194/wes-2025-265
Preprint. Discussion started: 8 December 2025

eawe european academy of wind energy
Open Access WIND ENERGY SCIENCE DISCUSSIONS

Conversely, dynamic WFFC techniques have not yet achieved a similar degree of maturity. The underlying principle of these strategies is to enhance the wake recovery through an improved mixing with the surrounding free stream flow, thus increasing the energy extraction of the downstream turbines (Meyers et al., 2022). In recent years, different concepts have been explored to achieve this effect, hence referred to as active wake mixing techniques. Munters and Meyers (2018) applied a sinusoidal signal to the thrust of the turbines, obtaining a pulsating wake. This method is referred to as dynamic induction control (DIC) or the pulse. Another promising technique named the helix approach was proposed by Frederik et al. (2020), who obtained considerable power gains by applying individual pitch control signals, obtaining a helical wake shape. These concepts have been proved through several LES studies (Taschner et al., 2023) and wind tunnel experiments (van der Hoek et al., 2024; Mühle et al., 2024), which have highlighted significant gains in power production but also increased structural loading on the turbines (Frederik and van Wingerden, 2022; van Vondelen et al., 2023).

Recent research has investigated the comparison between static and dynamic WFFC techniques through LES simulations, aiming to understand which solution ensures higher power production depending on the inflow conditions and the farm configuration. Taschner et al. (2024) have observed that the helix is favorable with respect to wake steering only in case of full wake overlap and up to six diameters of distance from the upstream turbine. However, they suggest that the combination between these methods could increase the robustness of the wind farm controller. This is a consequence of the abrupt change in the turbine yaw angle that occurs around the condition of full alignment with the downstream turbine. Frederik et al. (2025) and Brown et al. (2025) have shown that wake steering exhibits higher performance than wake mixing methods, except for inflow conditions characterized by low veer. Therefore, these studies have shown that wake mixing techniques seem to outperform the more mature wake steering method only in limited scenarios. However, their analysis has been limited to the effects within a two-turbines array and, therefore, these conclusions cannot be directly extended to large-scale wind farms. The main obstacle for the extension of such studies is the significant computational cost associated with multi-turbine LES simulations.

Large-scale wind farm simulations are usually performed through lower-fidelity steady-state wake models that allow a fast approximation of the wake characterization. These are often referred to as engineering wake models. In recent years, a wide variety of these models have been proposed and implemented in the popular software FLORIS (National Renewable Energy Laboratory, 2024a) and PyWake (Pedersen et al., 2023). Specifically, wake deficit models are combined with wake deflection models, such as Jimenez et al. (2010), to simulate the wind farm operation under yaw misalignment. Therefore, the low computational requirements of these models enable the optimization of the yaw angles for each turbine in large-scale wind farms, allowing the calculation of the increase in annual energy production (AEP) from wake steering. For instance, Simley et al. (2024) have applied these models to 15 different wind farms, calculating an AEP gain between $0.4\,\%$ and $1.7\,\%$ when wake steering is applied. Conversely, the literature lacks a comparable range of engineering models capable of simulating active wake mixing techniques. This is due not only to the lower technological maturity of these methods but also to the inherent difficulty of capturing their dynamic effects using steady-state models. Recently, National Renewable Energy Laboratory (2024a) has released a model named *Empirical Gaussian* which can simulate the effect of active wake mixing strategies by enhancing the wake recovery through a mixing factor. Dammann et al. (2025) have presented a model with similar capabilities using a Super

https://doi.org/10.5194/wes-2025-265
Preprint. Discussion started: 8 December 2025

eawe european academy of wind energy
Open Access WIND ENERGY SCIENCE DISCUSSIONS

Gaussian wake deficit model. Although these models enable a broader comparison and a potential integration of wake steering and active wake mixing, such a study has not yet been conducted on large-scale wind farms.

Another relevant aspect to consider when comparing and/or combining wake steering with active wake mixing is the uncertainty in the wind direction. This arises from different effects, such as the presence of turbulence and sensor errors (Quick et al., 2017), but also the spatial variation of wind direction in large wind farms neglected by engineering wake models (von Brandis et al., 2023). Brown et al. (2025) have shown that wake mixing techniques outperform wake steering in case of imperfect knowledge of the exact wake overlap position on the downstream turbine. Although the effect of such uncertainty remains unclear for active wake mixing techniques, this aspect has been studied extensively with respect to wake steering. Hodgson and Andersen (2025) demonstrated, through an LES study, that uncertainty in wind direction leads to a notable reduction in power gains. Quick et al. (2017) proposed an optimization under uncertainty to find the optimal yaw set-points. Rott et al. (2018) have evaluated a control strategy where wind direction uncertainty is integrated within the yaw optimization using realistic timeseries. In this case, a Gaussian probability density function is used to model the wind direction deviations and is obtained by fitting real measurements data. A similar approach has been adopted by Simley et al. (2020). The uncertainty in wind direction and its consequential unintentional yaw misalignments have been considered also for AEP calculation by some recent studies (Quick et al., 2020; van der Hoek et al., 2020). In general, wake steering energy gains have been shown to drop significantly when uncertainties in input conditions are considered (van Beek et al., 2021). For instance, van der Hoek et al. (2020) have estimated an AEP gain between $0.34\,\%$ and $0.60\,\%$ considering a standard deviation in the wind direction of 3° for a 60-turbines wind farm. However, including such uncertainty into the yaw angle optimization problem can yield more robust AEP gains, thereby mitigating its detrimental effects.

Lastly, a critical aspect of the application of WFFC in large-scale wind farms is the choice of the optimization algorithm to determine the control setpoints for the turbines. General gradient-based methods available in SciPy (Virtanen et al., 2020) or OpenMDAO (Gray et al., 2019) libraries can require extensive computational time as the number of turbines increases, or they could even encounter difficulties in reaching the global optimum. Fleming et al. (2022) have developed an algorithm for yaw angles optimization named Serial-Refine (SR). It is based on serial iterations from upstream to downstream turbines and represents a faster solution than traditional gradient-based methods. However, the SR algorithm has been developed specifically for wake steering, hence it cannot be directly applied when also active wake mixing techniques are considered.

In summary, previous studies have compared wake steering with active wake mixing techniques only for a limited number of turbines, while such comparison for large wind farms and the effect of a combined control strategy remain unexplored. This study addresses this problem by analyzing the effect of three different control methods: wake steering, the helix, and a combined strategy that allows each turbine to apply one of these two techniques. It investigates the added value of adopting such combined strategy for a large-scale wind farm, especially when uncertainty in wind direction is present.

The main contributions of this work are outlined as follows:

- Comparison between different WFFC strategies in terms of potential AEP increase for a large-scale wind farm.
- Sensitivity analysis for different degrees of wind direction uncertainty.

https://doi.org/10.5194/wes-2025-265
Preprint. Discussion started: 8 December 2025

eawe european academy of wind energy
Open Access WIND ENERGY SCIENCE DISCUSSIONS

Other additional contributions of this study can be summarized as follows:

- Development of a tailored algorithm to optimize the control setpoints of a combined control strategy, applicable to a generalized objective.
- Analysis of trade-off solutions through a multi-objective optimization approach based on an added penalty on the control effort.

The remainder of this paper is structured as follows. Section 2 outlines the methodology adopted in this study. Then, the results are presented in Sect. 3 and discussed in Sect. 4. Lastly, conclusion and recommendations for future research are included in Sect. 5.

2 Methodology

This section describes the methodology employed in this study, first explaining the wind farm model and the performance metrics selected as objectives. Then, the optimization problem to determine the control strategies is described, together with the optimization algorithm developed in this work. Lastly, the case studies chosen to showcase this framework are outlined.

2.1 Wind farm model

The turbines in the wind farm are modeled with their power and thrust curves. Dynamic effects are ignored and it is assumed that a change in wind speed is instantaneously transmitted to the power production. The effect of wake steering is modeled by reducing the incoming wind speed by $\cos\gamma$, with γ indicating the yaw misalignment. The power is then obtained from the corresponding power curve using the updated wind speed value. Similarly, the thrust coefficient C_T is also recalculated based on the updated wind speed value. However, it is further reduced by $\cos^2\gamma$ as defined by *Simple Yaw Model* implemented in the software PyWake (Pedersen et al., 2023). Among the different techniques for active wake mixing, only the helix approach has been modeled and considered in this study. Consisting of a sinusoidal signal, the main control variables of such technique are the excitation frequency, expressed through the Strouhal number St, and the blade pitch amplitude β (Frederik et al., 2020). The power P and thrust coefficient C_T are modeled as a function of their values during baseline operation, denoted by P_{BL} and $C_{T,BL}$, as

$$P(\beta) = P_{BL} \cdot [1 - (b_P + c_P \cdot P_{BL}) \cdot \beta^a] \quad , \tag{1}$$

and

$$C_T(\beta) = C_{T,BL} \cdot [1 - (b_T + c_T \cdot C_{T,BL}) \cdot \beta^a] \quad , \tag{2}$$

where a, b_P, c_P, b_T, and c_T are tuning coefficients that require proper tuning. In this study, the baseline operation is defined as the condition when WFFC is not applied. These equations follow the approach implemented in FLORIS (National

https://doi.org/10.5194/wes-2025-265
Preprint. Discussion started: 8 December 2025

eawe european academy of wind energy
Open Access WIND ENERGY SCIENCE DISCUSSIONS

Renewable Energy Laboratory, 2024a), where only the effect of a varying amplitude is considered while St is assumed to be optimal.

The wake deficit model used in this study is the *Empirical Gaussian* model implemented in FLORIS (National Renewable Energy Laboratory, 2024a) since it includes the effect of the added mixing induced by the helix control. The equations that describe the model are included in Appendix A and available in the FLORIS documentation, where an extensive explanation is provided. A unique characteristic of this model is the introduction of the "wake-induced mixing factor". This non-physical term is used instead of an explicit dependence on the turbulence intensity, and is affected when the helix method is activated, enhancing the wake recovery depending on β. For consistency, the *Empirical Gaussian* model is also adopted to determine the wake deflection caused by yaw or tilt misalignment. These models include several coefficients that have been tuned based on high-fidelity simulations to match the conditions that characterize the site of the selected case study. A detailed description of this process is included in Appendix A. Both the wake deficit and deflection models have been integrated within the software PyWake to conduct this study.

The wake deficits caused by multiple turbines are added in quadrature while the inflow wind speed over the rotor a turbine is calculated through numerical integration, following the approach of Pedersen et al. (2022). These methods are directly available in PyWake, designated as *Squared Sum* and *Gaussian Overlap*, respectively.

2.2 Performance metrics

The AEP of the wind farm is selected as the main performance metric. To provide a realistic AEP estimation, the calculation is performed considering the uncertainty in the wind direction. Specifically, this aspect is modeled by introducing some deviations from each value of wind direction that is simulated, without adapting the yaw angle of the turbines. This is achieved by including some offsets denoted by $\Delta\theta$ to the nominal wind direction, indicated with θ, and by weighting the power obtained for these multiple values of wind direction, i.e. $\theta + \Delta\theta$, using a probability distribution p_θ. In this case, a Gaussian function is used, defined by its standard deviation σ_θ and centered on the nominal wind direction. Then, the power P correspondent to a nominal flow condition (u, θ), with u indicating the wind speed, is obtained through the integration over the wind direction deviations, as indicated in Eq. (3). In the equation, f_P denotes the function that calculates the total power of the wind farm assuming $(u, \theta + \Delta\theta)$ as free-stream flow condition. Specifically, f_P performs the summation of the power outputs of the individual turbines, which are calculated based on the turbine and wake models described previously. Each nominal flow condition (u, θ) is associated with different values of control variables, denoted by $\boldsymbol{\gamma}$ and $\boldsymbol{\beta}$, which contain the yaw angles and helix amplitudes of each turbine. These are given as input to f_P, affecting the power production of the wind farm. Since the yaw angles are defined relative to the input wind direction, which in this case is $\theta + \Delta\theta$, they are adjusted by adding $\Delta\theta$ before being provided as input to f_P, simulating the unintentional misalignment.

$$P(\theta, u, \boldsymbol{\gamma}, \boldsymbol{\beta}, \sigma_\theta) = \int p_\theta(\Delta\theta, \sigma_\theta) \cdot f_P(\theta + \Delta\theta, u, \boldsymbol{\gamma} + \Delta\theta, \boldsymbol{\beta})\, \mathrm{d}\Delta\theta \tag{3}$$

https://doi.org/10.5194/wes-2025-265
Preprint. Discussion started: 8 December 2025

eawe european academy of wind energy
Open Access WIND ENERGY SCIENCE DISCUSSIONS

Lastly, the AEP is calculated by integrating the power P over the different values of wind speed u and direction θ weighted by their probability of occurrence $p(u,\theta)$, as shown in Eq. (4). The term $p(u,\theta)$ is derived from Weibull distributions specified for each wind direction at each turbine location. The spatial variability of these distributions captures the heterogeneous wind resources across the wind farm. The arguments $\boldsymbol{\gamma}_{\mathrm{LUT}}$ and $\boldsymbol{\beta}_{\mathrm{LUT}}$ included in the equation refer to the lookup tables (LUTs) containing the values of $\boldsymbol{\gamma}$ and $\boldsymbol{\beta}$ for each flow case (u,θ).

$$\mathrm{AEP}(\boldsymbol{\gamma}_{\mathrm{LUT}},\boldsymbol{\beta}_{\mathrm{LUT}}) = 8760\ \mathrm{h\,yr^{-1}} \cdot \iint p(u,\theta)\cdot P(\theta,u,\boldsymbol{\gamma},\boldsymbol{\beta},\sigma_\theta)\ \mathrm{d}u\ \mathrm{d}\theta \tag{4}$$

To gain insights on the control effort experienced by the turbines during their yearly operation, another performance metric is introduced in this work, named *control operation time* and denoted by COT. It quantifies the period during which each turbine operates under a WFFC strategy, i.e. yawing or applying the helix, and is is defined as follows. First, the control effort of turbine i, denoted with $c_{E,i}$, is defined for each flow case as a binary variable that specifies whether the turbine i operates under a WFFC strategy; therefore, as

$$c_{E,i} = \begin{cases} 1 & \text{if} \quad \gamma_i \neq 0 \text{ or } \beta_i \neq 0 \\ 0 & \text{otherwise} \end{cases} \tag{5}$$

where γ_i and β_i are the yaw angle and the helix amplitude of turbine i, respectively, for the specific flow case. Second, the control operation time of turbine i, indicated by COT_i, which expresses the operation under a WFFC strategy in terms of percentage of its total operating time, is defined as

$$\mathrm{COT}_i(\boldsymbol{\gamma}_{\mathrm{LUT},i},\boldsymbol{\beta}_{\mathrm{LUT},i}) = 100 \cdot \iint p(u,\theta)\cdot c_{E,i}(\gamma_i,\beta_i)\ \mathrm{d}u\ \mathrm{d}\theta \tag{6}$$

where $\boldsymbol{\gamma}_{\mathrm{LUT},i}$ and $\boldsymbol{\beta}_{\mathrm{LUT},i}$ refer to the values of $\boldsymbol{\gamma}_{\mathrm{LUT}}$ and $\boldsymbol{\beta}_{\mathrm{LUT}}$ of turbine i. Lastly, the control operation time of the wind farm, denoted by COT, indicates the average control operation time between the different turbines; hence defined as

$$\mathrm{COT}(\boldsymbol{\gamma}_{\mathrm{LUT}},\boldsymbol{\beta}_{\mathrm{LUT}}) = \frac{1}{N_{\mathrm{wt}}} \cdot \sum_{i=1}^{N_{\mathrm{wt}}} \mathrm{COT}_i(\boldsymbol{\gamma}_{\mathrm{LUT},i},\boldsymbol{\beta}_{\mathrm{LUT},i}) \tag{7}$$

While a high COT can guarantee a larger AEP, it also increases the complexity of the control strategy, which may limit its practical feasibility or raise concerns about higher structural loads. This issue is particularly relevant for the helix technique, as its operation is often associated with increased loads on several critical wind turbine components (Frederik and van Wingerden, 2022).

2.3 Wind farm flow control optimization problem

The control set points of each WFFC control strategy are calculated by solving an optimization problem. The results are the optimal yaw angles and helix amplitudes for each turbine and flow condition, indicated by $\boldsymbol{\gamma}_{\mathrm{LUT}}$ and $\boldsymbol{\beta}_{\mathrm{LUT}}$, respectively. This

https://doi.org/10.5194/wes-2025-265
Preprint. Discussion started: 8 December 2025

eawe european academy of wind energy
Open Access WIND ENERGY SCIENCE DISCUSSIONS

problem is divided into multiple sub-problems that are solved independently, each referring to a different flow condition (u, θ). The design variables of each sub-problem are the yaw angles $\boldsymbol{\gamma}$ and the helix amplitudes $\boldsymbol{\beta}$ of the turbines in the farm for the given flow condition (u, θ). Their values are limited within the bounds $[\gamma_{\min}, \gamma_{\max}]$ and $[\beta_{\min}, \beta_{\max}]$. In this study, each turbine is limited to use either wake steering or the helix, while different strategies are allowed for different turbines under the same flow conditions. This modeling choice is due to the lack of previous research and validation for cases where wake steering and helix are implemented on the same turbine simultaneously.

In this work, two different optimization problems are solved, differing by their objective function. The first problem is defined in Eq. (8), whose objective is to maximize the power production P, which considers the effect of wind direction uncertainty.

$$\begin{aligned} \underset{\boldsymbol{\gamma},\boldsymbol{\beta}}{\text{maximize}} \quad & P(\theta, u, \boldsymbol{\gamma}, \boldsymbol{\beta}, \sigma_\theta) \\ \text{subject to} \quad & \boldsymbol{\gamma} \in [\gamma_{\min}, \gamma_{\max}] \\ & \boldsymbol{\beta} \in [\beta_{\min}, \beta_{\max}] \end{aligned} \tag{8}$$

The second problem aims to both maximize the power production and minimize the control effort, hence adopting a multi-objective approach. The problem is described in Eq. (9), where the two objectives are combined through the weight w, which represents the relative importance of the two objectives.

$$\begin{aligned} \underset{\boldsymbol{\gamma},\boldsymbol{\beta}}{\text{maximize}} \quad & P(\theta, u, \boldsymbol{\gamma}, \boldsymbol{\beta}, \sigma_\theta) - w \cdot \sum_{i=1}^{N_{\text{wt}}} c_{E,i}(\gamma_i, \beta_i) \\ \text{subject to} \quad & \boldsymbol{\gamma} \in [\gamma_{\min}, \gamma_{\max}] \\ & \boldsymbol{\beta} \in [\beta_{\min}, \beta_{\max}] \end{aligned} \tag{9}$$

The problems described so far refer to the combined control strategy. In case of individual wake steering and helix strategies, the corresponding optimization problems differ only by the definition of the design variables, which in the former case are limited to $\boldsymbol{\gamma}$ and in the latter to $\boldsymbol{\beta}$.

2.4 Multi-strategy Serial-Refine (MSR) optimization algorithm

To solve the wind farm flow control optimization problems described in the previous section, a tailored optimization algorithm is developed, called Multi-strategy Serial-Refine (MSR) optimization algorithm. The algorithm aims to find the control strategy of a wind farm combining wake steering and active wake mixing to maximize a generic objective function. This algorithm is an extension of the SR optimizer developed by Fleming et al. (2022). The design variables are extended to consider several control strategies within a wind farm instead of only wake steering. Furthermore, the algorithm is adapted to allow an arbitrary objective function defined by the user.

Analogous to the SR method, the MSR algorithm iterates over each turbine from the most upstream to most downstream for each flow condition. At each iteration, a set of candidate control values is assessed for every turbine, and the best value

https://doi.org/10.5194/wes-2025-265
Preprint. Discussion started: 8 December 2025

eawe european academy of wind energy
Open Access WIND ENERGY SCIENCE DISCUSSIONS

Table 1. Settings and Hyperparameters of the MSR.

Number of values (N_{values})	5
Number of steps (N_{step})	3
Exclusivity	True
Bounds for yaw angle ($\gamma_{\min}, \gamma_{\max}$)	$[-30°, 30°]$
Bounds for helix amplitude ($\beta_{\min}, \beta_{\max}$)	$[0°, 5°]$

is selected. The subsequent iteration is then initialized by perturbing the previously selected control variables with decreasing offsets, thereby refining the solution space. Therefore, the algorithm is characterized primarily by two hyperparameters: the total number of iterations, N_{step}, and the number of candidate values evaluated per turbine, N_{values}. The main distinction from SR is the procedure applied at each turbine iteration. In this extended version, multiple control strategies are tested in parallel, and the best-performing one is selected. The exclusivity of the control strategy is enforced at the perturbation step: for each turbine, if a perturbation is applied for a given strategy, the control set point for the other strategy is set to zero. This feature is enabled through the hyperparameter *exclusivity*.

The settings and hyperparameters of MSR adopted for this study are included in Table 1, while a more detailed description of the optimization algorithm can be found in the Appendix B.

2.5 Case studies

Two case studies are considered to test the potential of a combined WFFC strategy. The first case study is a two-turbine wind farm where the wind direction and wind speed are kept constant, set to $270°$ and $8\,\mathrm{m\,s^{-1}}$, respectively. Whereas the position of the upstream turbine is fixed, different downstream and cross-stream distances are tested for the second turbine. This simple example is used to provide an intuitive understanding of the model and algorithm used in this work. The second case study is a large-scale offshore wind farm consisting of 69 turbine. This is a scaled version of the Hollandse Kust Noord (HKN) wind farm, obtained by preserving the distances between the turbines when normalized with their rotor diameter (D). The wind resources of the site are defined by the wind rose included in Fig. 1 and the heterogeneous wind speed field shown in Fig. 2 (Vortex FDC, 2024), where the layout of the wind farm is also reported. In this farm, the minimum distance between the turbines and the power density are $4.48\,D$ and $6.03\ \mathrm{W\,m^{-2}}$, respectively. For both case studies, the ambient turbulence intensity is set to 4% and the IEA $22\ \mathrm{MW}$ reference turbine (Zahle et al., 2024) is used, characterized by a diameter D of $283.2\ \mathrm{m}$.

The computation of the LUTs and the calculation of the performance metrics require the flow conditions to be discretized. Specifically, the wind speed and directions are discretized into bins of $1\ \mathrm{m\,s^{-1}}$ and $1°$, respectively. In addition, a bin size of $1.25°$ is used to solve the integral related to the wind direction uncertainty, shown in Eq. (3), calculated within the interval $[-2\sigma_\theta, 2\sigma_\theta]$. Table 2 summarizes the main characteristics of the second case study.

https://doi.org/10.5194/wes-2025-265
Preprint. Discussion started: 8 December 2025

eawe european academy of wind energy
Open Access WIND ENERGY SCIENCE DISCUSSIONS

Table 2. Main characteristics of the scaled HKN case study.

Number of turbines	69
Turbine type	IEA 22 MW
Minimum distance	4.48 D
Power density	6.03 $\mathrm{W\,m^{-2}}$
Wind direction bin size	1°
Wind speed bin size	1 $\mathrm{m\,s^{-1}}$

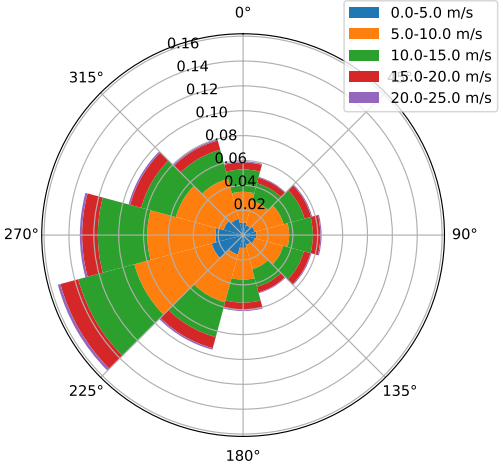

Figure 1. Wind rose of Hollandse Kust Noord site (Vortex FDC, 2024).

In this work, three selected values of σ_θ are used to test the effectiveness of the WFFC strategies under various conditions. These are $0°$, i.e. no uncertainty, $2.5°$, and $5°$. In the literature, standard deviation values up to $5.25°$ have been utilized, often extracted from measurement data (Rott et al., 2018).

Within this study, the effects of the different WFFC strategies are evaluated in comparison to a baseline case, defined as the condition in which all control variables included in the LUTs are set to zero, corresponding to a greedy operation of the wind farm.

3 Results

This section describes the results of the analysis conducted in this study. First, the capabilities of the combined control strategy are shown for the two turbines example. Second, the results of the scaled HKN case study are described in terms of increase in AEP, description of the optimal control variables, impact on COT, and trade-offs obtained with the multi-objective approach.

https://doi.org/10.5194/wes-2025-265
Preprint. Discussion started: 8 December 2025

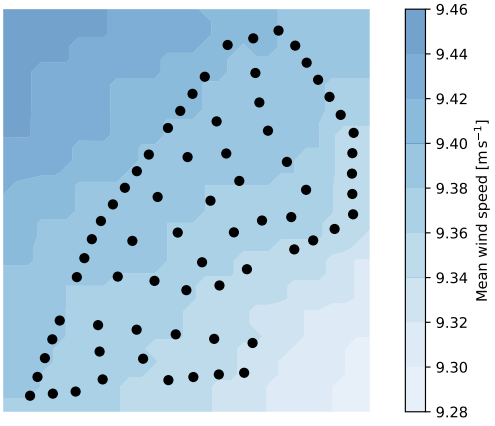

Figure 2. Location of the turbines and heterogeneous mean wind speed map at Hollandse Kust Noord site.

3.1 Two turbines example

This section outlines the results for the case study consisting of two turbines. The optimal control variables of the front turbine are calculated for different positions of the downstream turbine and are shown in Fig. 3. These are obtained by solving the optimization problem depicted in Eq. (8), based on power maximization. The first turbine is positioned at the origin of each plot, $(0, 0)$. The second turbine is placed at varying downstream and cross-stream distances, denoted by dx and dy, respectively. These distances are normalized by D and shown on the axes.

Nine different cases are presented, namely the three WFFC strategies, wake steering, helix, and combined, for three values of uncertainty in wind direction, i.e. $\sigma_\theta \in [0°, 2.5°, 5°]$. It can be observed that, as the uncertainty in the wind direction increases, the downstream area for which the control is activated gets larger. However, the magnitude of the control variable diminishes, leading to a less aggressive strategy. This happens irrespective of the type of the WFFC strategy.

Analyzing the combined control strategy, for $\sigma_\theta = 0°$ there is only a very narrow region where the helix is superior than wake steering. This condition only occurs in case of perfect alignment between the two turbines and up to a limited distance, as demonstrated also by Taschner et al. (2024). Therefore, for this simplified example and in case the uncertainty in the wind direction is neglected, a combined control strategy would not differ significantly from only using wake steering. However, as the uncertainty in the wind direction increases, the region where the helix outperforms wake steering becomes larger, showing added value of the combined strategy.

Figure 4 shows the power gains corresponding to the optimal control strategy depicted in Fig. 3. These are defined as the percentage difference in wind farm power production between the case when WFFC is activated and the baseline operation. From Fig. 4, it can be observed that the power gains achieved through WFFC decrease as the uncertainty in wind direction increases. This detrimental effect appears to be more pronounced for wake steering than for the helix strategy. In most cases,

https://doi.org/10.5194/wes-2025-265
Preprint. Discussion started: 8 December 2025

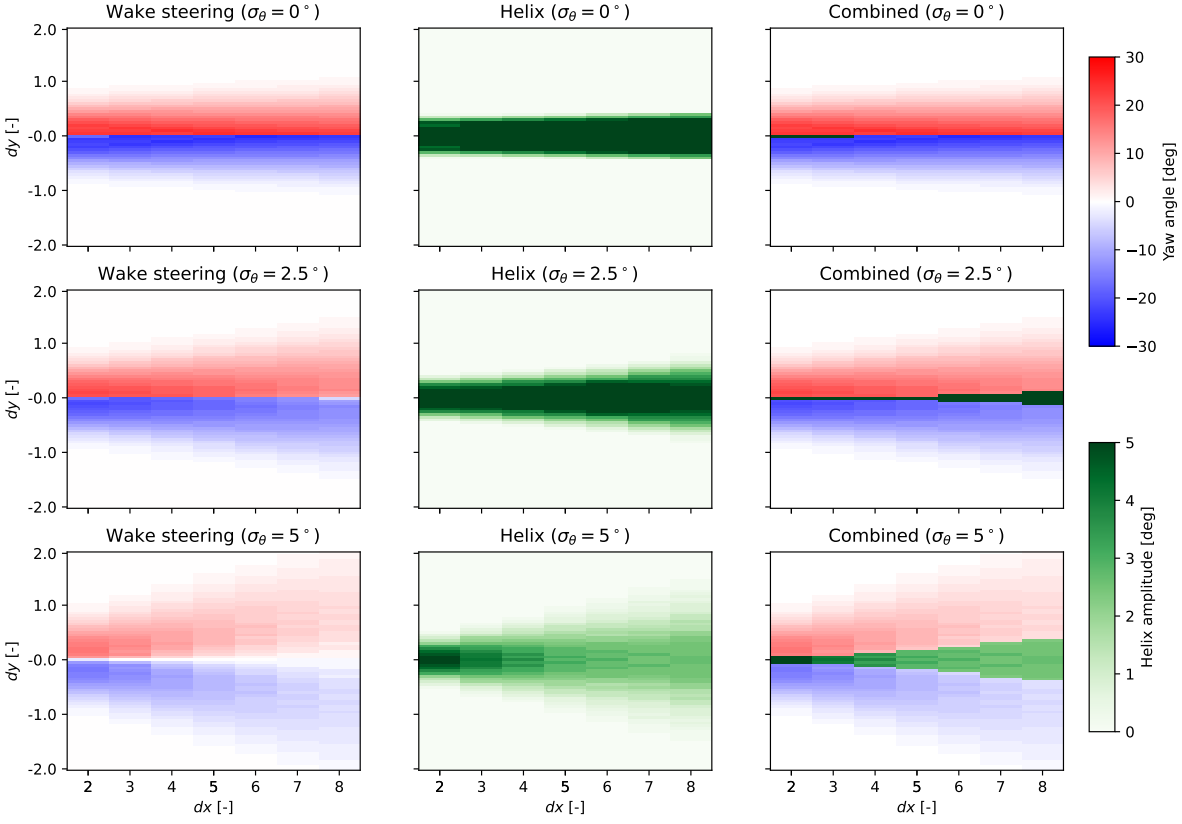

Figure 3. Optimal yaw angle and helix amplitude of the upstream turbine for different positions of the downstream turbine in a farm consisting of two turbines. The position of the downstream turbine in expressed in terms of streamwise and cross-stream distances from the upstream turbine, normalized with D. The wind speed and direction are $8\ \mathrm{m\,s^{-1}}$ and 270°, respectively. Each subplot is characterized by a different control strategy and degree of uncertainty in wind direction, both specified in each subtitle.

the power gains obtained with wake steering are higher than those achieved with the helix in most cases. Furthermore, the plots corresponding to the combined control strategy closely resemble those obtained by using wake steering alone. Overall, from these results, it can be concluded that wake steering significantly outperforms the helix in the partial-overlap case. Conversely, the helix yields slightly higher power gains under fully aligned conditions; however, this difference remains marginal.

https://doi.org/10.5194/wes-2025-265
Preprint. Discussion started: 8 December 2025

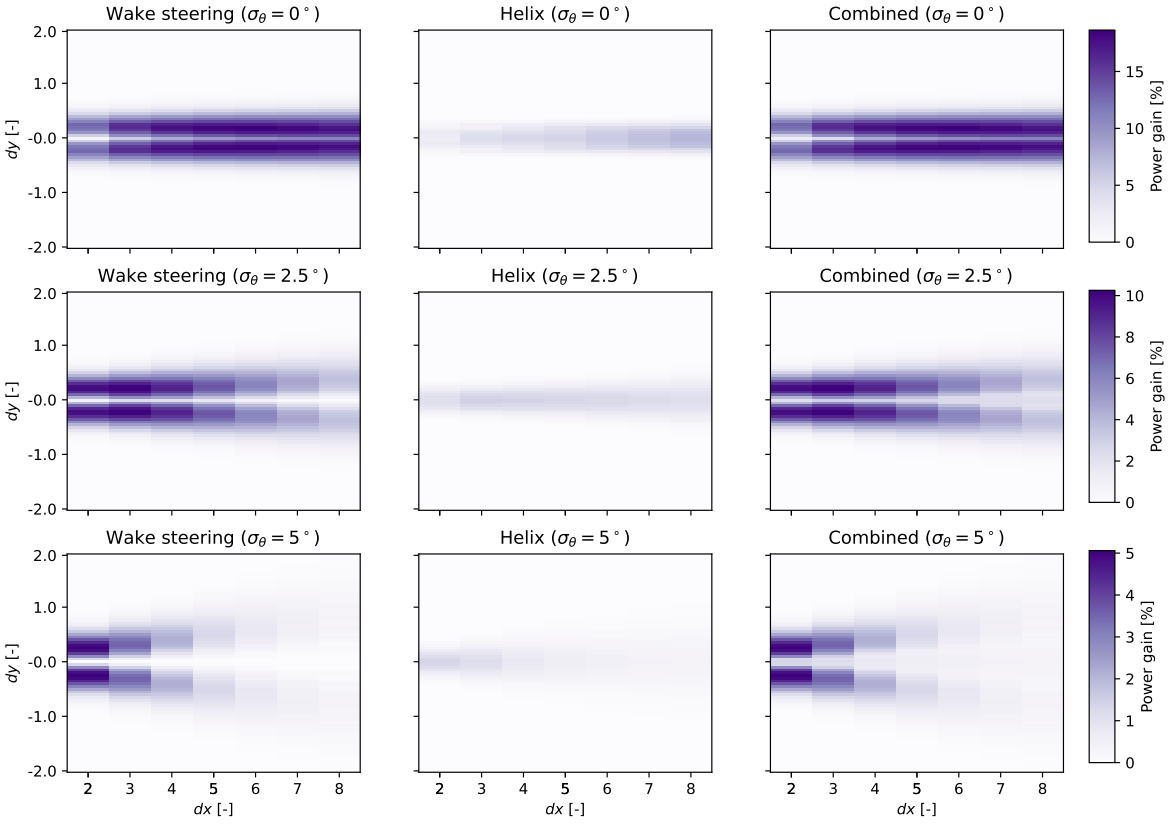

Figure 4. Power gains of the two turbines wind farm for different positions of the downstream turbine. The wind speed and direction are $8\,\mathrm{m\,s^{-1}}$ and 270°, respectively. Each subplot is characterized by a different control strategy and degree of uncertainty in wind direction, both specified in each subtitle.

3.2 Large-scale wind farm

This section outlines the results concerning the large-scale wind farm case study, for which the different WFFC strategies are applied to a scaled version of the HKN wind farm.

3.2.1 Increase in annual energy production

This section focuses on the impact of the combined strategy on the AEP of the wind farm. For this case study as well, the LUTs of optimal control variables are calculated to maximize the power production, as represented by Eq. (8). Different LUTs are

https://doi.org/10.5194/wes-2025-265
Preprint. Discussion started: 8 December 2025

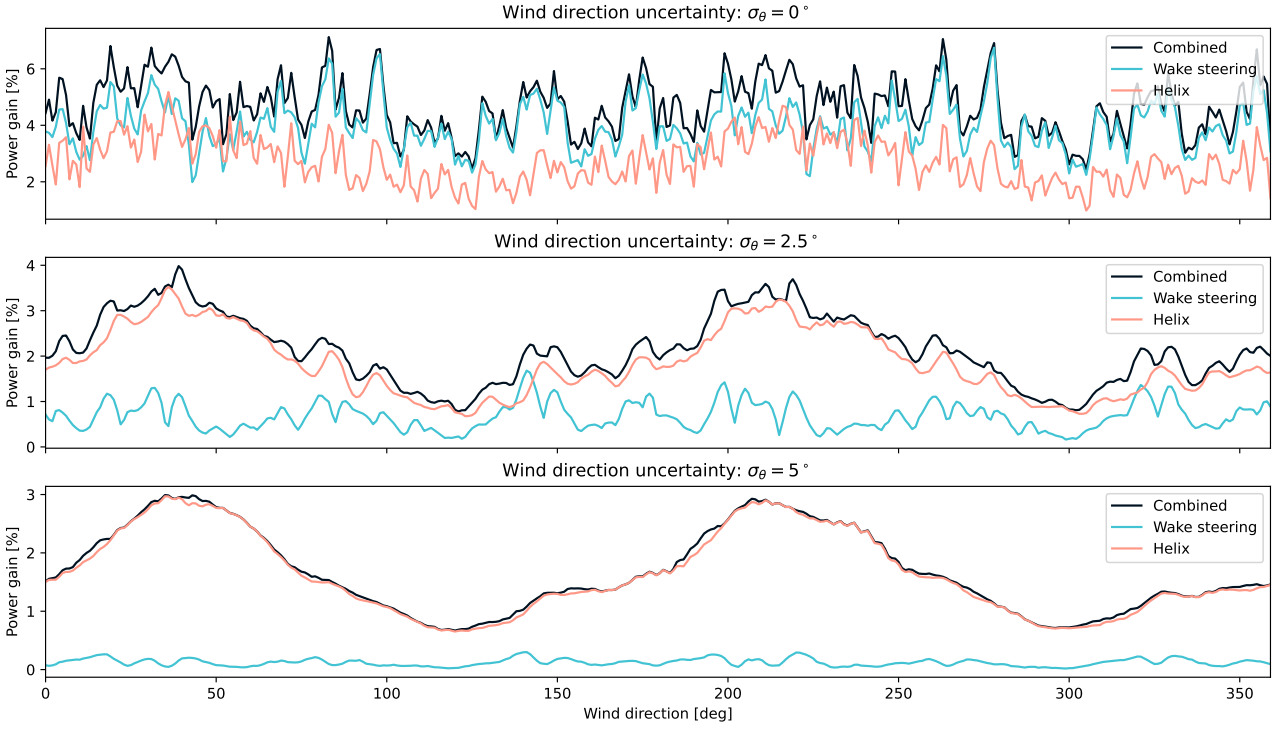

Figure 5. Power gains with respect to baseline operation of the scaled HKN wind farm for different wind directions. The figure includes different control strategies (indicated by different colors) and different degrees of uncertainty (specified in the subtitle of each plot). These values refer to a wind speed of $8\,\mathrm{m\,s^{-1}}$.

obtained for three levels of wind direction uncertainty, namely $\sigma_\theta \in [0^\circ, 2.5^\circ, 5^\circ]$. The results presented in this section show the increase in power production and AEP obtained applying wake steering, the helix and the combined strategy.

Figure 5 shows the power gains of the wind farm for each control strategy as a function of the wind direction, for a wind speed of $8\,\mathrm{m\,s^{-1}}$. It can be observed that the magnitude of the power gains vary across the strategies, with the combined strategy showing the highest power gains for all cases. When the wind direction uncertainty is neglected ($\sigma_\theta = 0^\circ$), Fig. 5 shows that wake steering provides higher gains with respect to the helix, similarly to the two turbines case study. As a consequence, wake steering is adopted by most of the turbines also for the combined strategy. Therefore, the gains of the combined strategy are almost aligned with the values provided by wake steering. However, a different behavior is observed as σ_θ increases. For $\sigma_\theta = 2.5^\circ$, the situation is reversed, namely the helix outperforms wake steering. Therefore, the power increase provided by the combined control strategy is closer to the values obtained by the helix operation. This trend further increases when $\sigma_\theta = 5^\circ$, for which the benefits of wake steering are significantly lower with respect to the helix.

Lastly, to assess the performance of the different control strategies, the AEP values are calculated. Their values are expressed in terms of percentage difference with respect to the baseline operation, thereby providing a quantitative estimate of the benefits of the WFFC strategies over the lifetime of the wind farm. The results are reported in Fig. 6. As observed previously, the wind

https://doi.org/10.5194/wes-2025-265
Preprint. Discussion started: 8 December 2025

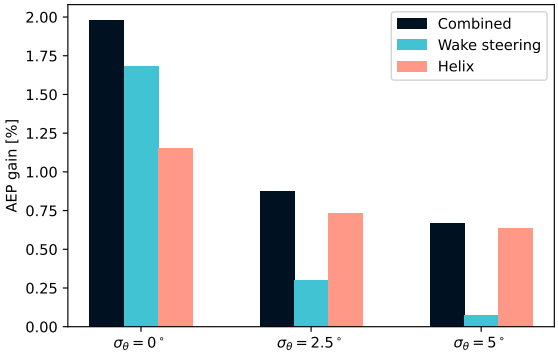

Figure 6. AEP gains with respect to baseline operation of the scaled HKN wind farm. The figure includes different control strategies (indicated by different colors) and different degrees of uncertainty (specified in the x-axis).

direction uncertainty has a substantial unfavorable impact on the effectiveness of WFFC, regardless of the control strategy. This effect is highly pronounced for wake steering, where the AEP gain drops from $1.68\,\%$ to $0.30\,\%$ and $0.07\,\%$, corresponding to values of σ_θ equal to $0°$, $2.5°$, and $5°$, respectively. Conversely, Fig. 6 demonstrates that the AEP gains obtained applying the helix are more robust with respect to wind direction uncertainty. Despite a lower AEP gain ($1.15\,\%$) for $\sigma_\theta = 0°$, it diminishes to $0.73\,\%$ and $0.63\,\%$. Lastly, the combined strategy exhibits a high AEP gain ($1.98\,\%$) if $\sigma_\theta = 0°$, relying mostly on wake steering, while limiting the drop to $0.88\,\%$ and $0.67\,\%$ by exploiting the robustness of the helix.

3.2.2 Lookup tables of the combined strategy

This section examines the control variables in the LUTs that yielded the power and AEP gains reported in the previous section. The plots are presented to show the optimal control settings required to achieve these gains, in order to reveal general trends and to evaluate the practical feasibility of implementing such control strategies. The results are shown for two representative cases: a turbine located at the farm boundary and one situated at its center. The optimal control values are depicted using a "control rose", which displays the control variables as a function of wind speed and direction.

Figure 7a shows the control rose of one turbine in the front row facing the dominant wind direction, whose position is highlighted in the same figure. This refers to the LUTs of the combined control strategy, obtained for $\sigma_\theta = 2.5°$. It can be observed that this turbine applies wake steering only when the wind direction is oriented with the wind farm boundaries, where many turbines are aligned. Therefore, wake steering is activated only when the turbine is able to deviate its wake from the majority of the downstream turbines, and this condition cannot be achieved if the wake is facing the central region of the wind farm. Conversely, the helix operation is activated when the wake of the turbine impacts exactly this region, where multiple turbines are present but not aligned along one specific direction. This occurs because, rather than redirecting the wake toward

https://doi.org/10.5194/wes-2025-265
Preprint. Discussion started: 8 December 2025

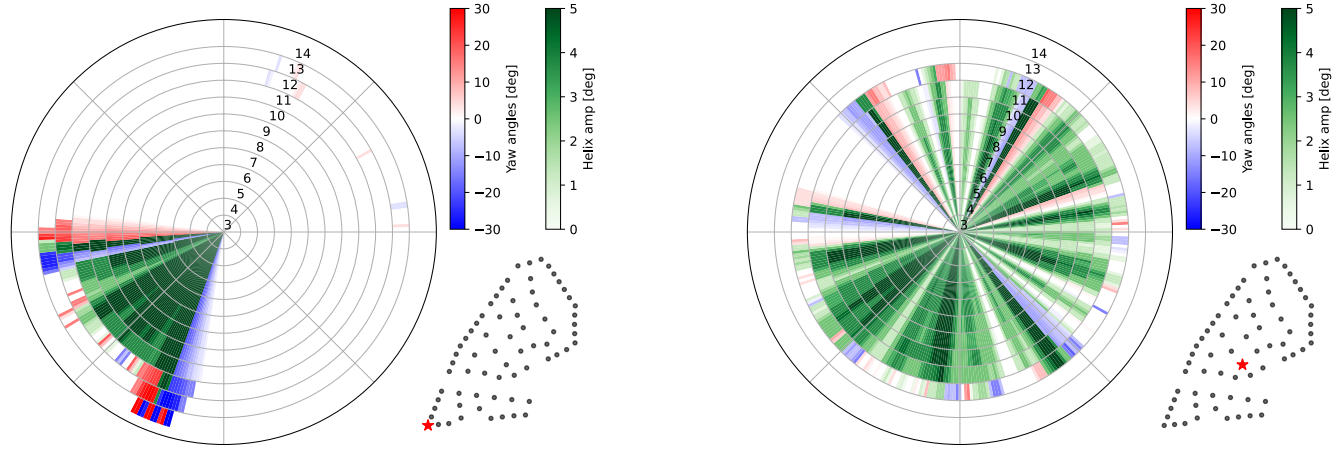

(a) Turbine located at the boundaries of the farm.

(b) Turbine located in the central region of the farm.

Figure 7. Control rose for the combined strategy of two different turbines. The exact position of the turbines are highlighted in the wind farm layout included in each subplot. Each subplot includes the values of the control variables present in the LUT for each wind speed and direction, obtained for a wind direction uncertainty $\sigma_\theta = 2.5^\circ$.

other turbines, the wind speed deficit is reduced due to enhanced mixing. Therefore, the two control strategies are used for this turbine to mitigate the wake effect for different flow conditions, showing good complementarity.

Figure 7b illustrates the control rose of a turbine that is placed in the central region of the wind farm. The results indicate that the control strategy of this turbines mainly consists of applying the helix technique, with wake steering being activated for few limited cases. Specifically, it can be observed that the helix is activated on this turbine for even broader set of conditions with respect to the turbine located on the boundaries of the farm. The same explanation provided for the previous turbine still holds, i.e. helix control is favorable when multiple misaligned turbines are present in the wake. However, the aggressive control strategy of this turbine would probably not contribute significantly to the increase in AEP observed for the wind farm. This motivates a deeper analysis on the COT of the turbines, described in the next sections.

3.2.3 Impact on the control operation time

This section investigates the impact of the different control strategies in terms of control operation time. Figure 8 reports the control operation time of each individual turbine, i.e. COT_i. The values are shown using boxplots, which summarize the main trends across the turbines for each condition. It can be observed that the values of COT_i can differ significantly depending on the turbine, as highlighted by the vertical length of each "box". Moreover, different values of COT_i are obtained depending both on the control strategy and the level of uncertainty. However, the main observation from Fig. 8 is that some turbine would operate under either wake steering or helix mode for more than $60\,\%$ of the time. In case of the helix, this could lead to a significant increase in the structural loading, preventing the feasibility of such control strategy. These results can be explained based on the problem statement in Eq. (8), where the use of control is not penalized. As a result, the use of WFFC is encouraged

https://doi.org/10.5194/wes-2025-265
Preprint. Discussion started: 8 December 2025

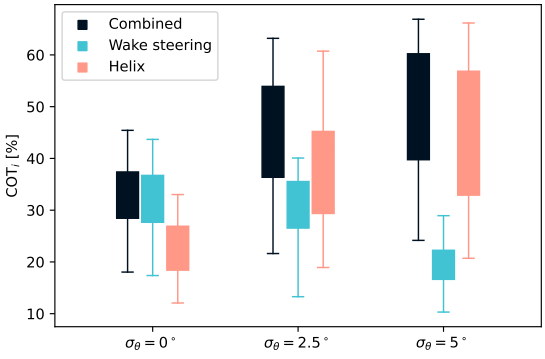

Figure 8. Control operation time for different control strategies (indicated by the color) and wind direction uncertainty (specified in the x-axis). Each boxplot summarizes the values of all the turbines in the wind farm for the specific condition.

even if only a minimal gain in power production is obtained. Moreover, two additional aspects can be observed in Fig. 8. First, the effect of wind direction uncertainty on COT_i depends on the control strategy. Figure 8 highlights a direct correlation with σ_θ for the helix and the combined strategy, while an inverse trend is observed for wake steering. Second, the values of COT_i related to the helix and the combined strategy are significantly higher than for wake steering when uncertainty in wind direction is considered. An explanation to this result can be provided by assuming that several turbines present a LUT similar to the one depicted in Fig. 7b. In this case, the turbines apply either wake steering or the helix for most of the flow conditions below rated wind speed, which represent a significant fraction of the total operation time.

3.2.4 Multi-objective

A multi-objective approach is conducted to balance the gains in power production provided by the different control strategies and their associated control effort, as described in Eq. (9). The results are shown in Fig. 9, where the effect of different LUTs are included in terms of AEP gain and COT. Each data-point in the Pareto front corresponds to a different LUT, with its associated performance metrics. The different values that determine each curve are obtained by increasing the weighting of the penalty on the control effort present in the objective function. Specifically, the Pareto fronts have been obtained by varying the weight w from 0 to 10^6. The results are shown for the three different control options investigated in this study, assuming $\sigma_\theta = 2.5°$. Moreover, two additional cases have been included, where $\beta_{\max}$ in the helix and the combined strategies has been limited to $2.5°$, in contrast to the value of $5°$ adopted in the rest of the study. This provides a wider overview on the potential of these techniques, quantifying the impact of a less aggressive helix operation, for instance due to constraints on the structural loads (Frederik and van Wingerden, 2022; van Vondelen et al., 2023).

All the Pareto fronts represented in Fig. 9 show the presence of a trade-off between AEP and COT. The AEP gains are higher for the combined strategy compared to the individual strategies, in alignment with previous results. However, the high steepness

https://doi.org/10.5194/wes-2025-265
Preprint. Discussion started: 8 December 2025

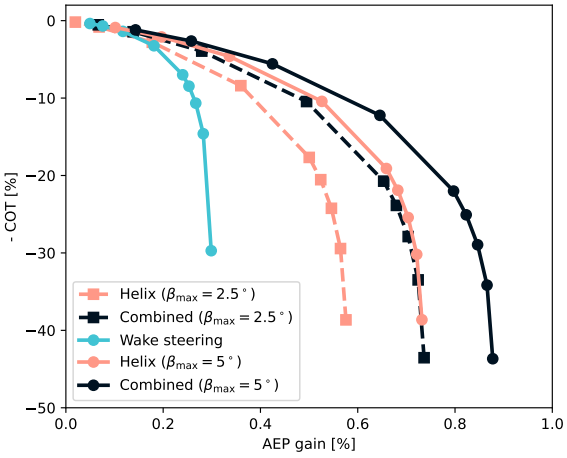

Figure 9. Trade-off between AEP gains and COT, for wake steering, helix and combined strategy, and for a maximum helix amplitude $\beta_{\max}$ of 5° and 2.5°. The results refer to a wind direction uncertainty of 2.5°.

of the Pareto fronts in proximity of the largest AEP gains indicates that beneficial trade-offs can be achieved. For instance,the COT of the combined can be limited to $22.0\,\%$ while keeping the AEP gain equal to $0.80\,\%$, obtained for $w = 10^5$. When $\beta_{\max}$ is limited to 2.5°, a shift in the Pareto curve is observed. In this case, a combined control strategy that aims a favorable trade-off between the two objectives can increase the AEP by $0.65\,\%$ while keeping COT to $20.73\,\%$. Similar trends can also be observed for wake steering and the helix. Overall, this analysis shows that a significant reduction in the COT can be achieved at the expense of only a marginal decrease in the AEP gain, and that even in this case, the combined strategy outperforms the individual techniques.

4 Discussion

This section provides a more detailed interpretation of the results obtained in this study, highlighting both their significance and limitations.

4.1 Insights on the comparison between different strategies

The comparison between wake steering and the helix has proved the superiority of the former when perfect inflow knowledge is used. However, the latter becomes favorable if uncertainty in wind direction is introduced, hence when more realistic conditions are simulated. This is a consequence of the asymmetric profile of optimal yaw angles with respect to the direction of full alignment with the downstream turbine, which represents a point of discontinuity. In the proximity of this condition, the optimal yaw angles oscillate from positive to negative large values, as clearly shown in Fig. 3. Therefore, in the absence of a

https://doi.org/10.5194/wes-2025-265
Preprint. Discussion started: 8 December 2025

well-defined misalignment direction, wake steering may be detrimental to power production. Conversely, such behaviour is not present for the helix operation, where a symmetric profile is observed.

This effect is amplified as the size of the wind farm increases. In many cases, having multiple downstream turbines prevents the upstream turbine to effectively steer the wake away from them. This condition occurs when the wake of the upstream turbine affects the central region of the farm, while the use of wake steering remains extremely fruitful when the upstream manages to redirect the wake towards outside the entire farm. In contrast, the helix technique does not exhibit this effect, as it reduces the wind speed deficit rather than displacing it. Therefore, the advantages of the helix approach emerge more clearly when a large-scale wind farm is considered instead of a limited number of turbines. These insights are expected to hold for wind farms characterized by a similar number of turbines, layout, and power density to our case case study; however, these trends may vary for other types of wind farm.

In this study, only the helix technique is used as active wake mixing strategy. However, the same framework can be used to study the impact of other techniques such as the pulse, for which Frederik et al. (2025) have demonstrated superior performance for some flow cases. This would only involve minor changes in the turbine model and the re-tuning of some coefficients that characterize the wake model. However, since the steady-state effects are expected to be similar to those observed for the helix, similar trends are also expected irrespective of the specific active wake mixing technique employed.

4.2 Reliability of low-fidelity wind farm models

The magnitude of the AEP gains mentioned in this study is highly dependent on the low-fidelity models that are used, especially on their coefficients. For instance, the power–yaw loss exponent, which is usually adopted to calculate the drop in power production due to an operation under yaw misalignment (Liew et al., 2020), can significantly affect the effectiveness of wake steering and its use within the combined strategy. In this study, the default method available in PyWake is used, based on the cosine loss law for the wind speed and the extraction of the updated power from the power curve of the turbine based on this wind speed value. In our case, this results in a power–yaw loss exponent between 2.5 and 3.1, depending on the wind speed. Conversely, Liew et al. (2020) have proved that the actual power–yaw loss exponent can be lower. Consequently, decreasing such value would lead to higher power gains for wake steering. As a results, wake steering would be adopted for a higher number of cases within the combined strategy, increasing the overall AEP gain. However, this would not affect the general trends presented in this work.

Overall, the coefficients adopted for these models have been tuned through aeroelastic simulations and LES to replicate the conditions of a realistic site. Nevertheless, the recent models used to consider the effect of the active wake mixing technique require additional validation to ensure reliability. Specifically, the scale of the LES simulations used for validation should be extended from a few turbines to larger wind farms to investigate the deep array effects and avoid extrapolation beyond validated conditions. An example of these limitations is the synchronization concept for the helix operation in multiple turbines. In this regard, recent studies have highlighted that synchronizing the wake dynamics of multiple turbines performing the helix may affect significantly the power production (van Vondelen et al., 2025). As of now, this aspect is neglected by the low-fidelity models currently available and, therefore, not considered in this study. Lastly, data from field experiments are needed to further

https://doi.org/10.5194/wes-2025-265
Preprint. Discussion started: 8 December 2025

improve the reliability of low-fidelity models in simulating wake mixing effects and to prove the effectiveness of active wake mixing strategies.

4.3 Implications of estimating the AEP using LUTs

In this study, the benefits of the different control strategies is estimated using LUTs, which contain the optimal control variables for each specific flow condition. Such estimation is typically performed under the assumption of a perfect knowledge of the wind direction ($\sigma_\theta = 0$), thereby simulating the exact flow conditions for which the control variables in the LUTs were derived. Such assumptions could lead to an overestimation of the AEP gains provided by the control strategies, due to the dynamic inflow conditions under which the turbines operate. Specifically, this assumption would require the control settings to be updated continuously to match the values contained in the LUTs. In this work, such assumption is relaxed by increasing the value of σ_θ, simulating more realistic conditions.

The use of LUTs for estimating the AEP does not imply that they are employed in the actual operation of the wind farm. In the context of AEP estimation, the LUTs assume that the optimal control variables are applied by the operator under each flow condition defined by u and θ, subject to an error margin determined by the wind direction uncertainty. However, the manner in which these control settings are implemented in response to dynamic flow conditions does not need to match the way the AEP is calculated to keep the estimation valid. For instance, the control setpoints may be applied through a combination of LUTs and a low-pass filter, or via more advanced closed-loop control strategies (Becker et al., 2025b).

In this context, the interpretation of the wind direction uncertainty is twofold. First, it estimates the impact of undesired effects such as sensor errors or rapid changes in wind conditions. Second, it reflects the behavior of a control approach designed to minimize actuator interventions, maintaining unaltered the control settings across a wider range of inflow conditions (Becker et al., 2025a).

While the decoupling between AEP estimation and the implementation of the actual operational strategy ensures broad applicability of the proposed method, it also raises concerns regarding the practical feasibility of deploying the combined control strategy. As previously noted, this strategy entails that certain turbines operate under wake steering, while others apply the helix technique, excluding the simultaneous application of both methods on a single turbine. This study has highlighted that switching between these two strategies for different inflow conditions can lead to a substantial increase in power production. However, how this transition can be executed under the actual operation remains unexplored and requires validation based on LES and wind tunnel experiments. Lastly, the helix's performance under yaw misalignment remains largely unexplored, yet it may offer further AEP improvements and thus merits detailed investigation.

4.4 Impact of the flow characteristics

In this work, the flow characteristics have been selected to replicate the site conditions of the case study. However, Frederik et al. (2025) have shown that the veer has a significant impact on selecting the best control strategy. Therefore, a sensitivity analysis on the veer value would provide a wider overview on the comparison between the different control options tested in this study.

https://doi.org/10.5194/wes-2025-265
Preprint. Discussion started: 8 December 2025

The turbulence intensity is also expected to play a major role in the comparison and combination of different WFFC techniques. However, the Empirical Gaussian wake model adopted in this study does not present any explicit dependencies on such parameters, relying completely on the tuning process. Therefore, the coefficients of the model would need to be re-tuned for each value of turbulence intensity that is investigated, requiring an extensive dataset of LES simulations representing all these conditions. Therefore, the development of a wake model for active wake mixing with a direct dependence on the turbulence intensity would facilitate this analysis.

After completing all these sensitivity studies, multi-dimensional LUTs could be obtained by applying the framework developed in this work, where the optimal control variables are selected for all the possible combinations of the flow parameters.

4.5 Towards a value-centered wind farm flow control

The framework and the algorithm developed in this study have been devised to guarantee high flexibility in terms of the objective function to determine the optimal control strategy. Therefore, the optimization of the WFFC strategy can be extended beyond the traditional power production, exploring different value-based metrics (Meyers et al., 2022).

In this study, this concept has been showcased by balancing the annual energy production with the control operation time. In case of the helix operation, this variable can be directly related to an increased structural loading (Frederik and van Wingerden, 2022), while for wake steering the relation between these two aspects is more complex. A first attempt to better capture the information about the increased loads can be to penalize the control operation depending on the effective wind speed value and the magnitude of the control variable, i.e. yaw angle and helix amplitude values. Alternatively, load surrogate models can be integrated in this framework to provide better results with respect to power-loads trade-off strategies. For instance, Guilloré et al. (2024) proposed a surrogate model based on an artificial neural network that enables a rapid load estimation, while Anand et al. (2025) adopted this model to demonstrate the use of WFFC including lifetime-aware considerations. However, this model does not support active wake mixing control strategies yet.

Although most of this work has focused on maximizing the power production, the main objective could be shifted to the revenues generated by the wind farm using the same method and algorithm. This is expected to further increase the benefits of WFFC when wind speed and electricity prices are negatively correlated (Bechmann and Quick, 2025). This is a consequence of the fact that WFFC is mostly applied in the below-rated region, i.e. for low values of wind speed that are often associated to higher electricity prices.

Lastly, the proposed methodology and the developed algorithms can be applied to study the impact of WFFC beyond commercial metrics, including environmental, ecological, and/or social objectives within the wind farm flow control optimization problem (Meyers et al., 2022; Kainz et al., 2025).

5 Conclusions

This study has analyzed the added value of using a wind farm flow control strategy that combines wake steering with active wake mixing, with a specific focus on the helix technique. This combined strategy has demonstrated to increase substantially

https://doi.org/10.5194/wes-2025-265
Preprint. Discussion started: 8 December 2025

eawe european academy of wind energy
Open Access WIND ENERGY SCIENCE DISCUSSIONS

the power production of large-scale wind farms, achieving an AEP gain up to $1.98\,\%$, which exceeds the gains of $1.68\,\%$ and $1.15\,\%$ obtained individually for wake steering and the helix, respectively.

An increase in wind direction uncertainty has resulted in a significant drop in performance for all the different control strategies. However, this detrimental effect is more evident for wake steering, whose gains in AEP decrease to $0.30\,\%$ and $0.07\,\%$, corresponding to an uncertainty of $2.5°$ and $5°$, respectively. On the other hand, the helix has registered a drop to $0.73\,\%$ and $0.63\,\%$ for the same values of uncertainty. The uncertainty in wind direction also affects the combined strategy, resulting in AEP gains of $0.88\,\%$ and $0.67\,\%$, depending on the magnitude of the uncertainty. This outcome is a consequence of the high gains provided by wake steering for few favorable conditions and the high robustness of the helix with respect to wind direction uncertainty together with its applicability when multiple misaligned downstream turbines are present. However, such performance would require some turbines to operate under a WFFC strategy up to $60\ \%$ of their operation time, raising concerns on its actual feasibility. A multi-objective approach that balances the control effort with the increase in the power production has been adopted for the optimization of the control variables. For a wind direction uncertainty of $2.5°$, the control operation time can be reduced to $22.0\,\%$ while keeping the AEP gain to $0.80\,\%$.

This analysis has been enabled by the development of a tailored algorithm named MSR, which has been developed with the scope of providing high flexibility to the user, both in terms of control strategies and optimization objectives.

However, these results are based on recent wake models used for wind farm simulation, which are associated with notable uncertainties. Future research could diminish such uncertainty through a more extensive validation of the engineering models for active wake mixing, performing LES for large-scale wind farms, wind tunnel tests, and/or field experiments. Moreover, a wider variety of flow conditions could be simulated, providing comprehensive lookup tables of optimal control settings, depending also on parameters such as turbulence intensity or veer. Lastly, the full potential of this framework could be exploited by extending the analysis to the combination of more control strategies, e.g. including turbine derating, and more objectives, for instance related to structural, financial, environmental, ecological, and/or social aspects.

Code and data availability. https://github.com/matteobaricchi/msr

Appendix A: Description and tuning of the turbine and wake models

This appendix provides a description of the *Empirical Gaussian* wake deficit and deflection models, as well as the tuning procedure used for the turbine and wake models.

A1 Description of the Empirical Gaussian model

The *Empirical Gaussian* model adopted in this study is extensively described in FLORIS documentation (National Renewable Energy Laboratory, 2024a), however, the main equations are reported here as well.

The normalized wind speed at the point (x, y, z) is expressed as

https://doi.org/10.5194/wes-2025-265
Preprint. Discussion started: 8 December 2025

eawe european academy of wind energy
Open Access WIND ENERGY SCIENCE DISCUSSIONS

$$\frac{u}{U_\infty} = 1 - C \cdot \exp\left[-\frac{(y-\delta_y)^2}{2\sigma_y^2} - \frac{(z-\delta_z)^2}{2\sigma_z^2}\right] \tag{A1}$$

where the scaling factor C of the Gaussian curve and the lateral wake width σ_y depend on the downstream position x of the point at which the wind speed is evaluated, and are modeled as

$$C = \frac{1}{\sigma_{0,D}^2} \cdot \left(1 - \sqrt{1 - \frac{\sigma_{y,0}\sigma_{z,0}C_T}{\sigma_y\sigma_z}}\right) \quad , \tag{A2}$$

and

$$\sigma_y(x) = \sigma_{y,0} + \int_0^x \left[\sum_{i=0}^{n} k_i \cdot l_{[b_i,b_{i+1})}(x') + w_v \cdot M_j(x')\right] dx' \quad , \tag{A3}$$

respectively. The vertical wake width σ_z is defined similarly to σ_y, hence following Eq. (A3). δ_y and δ_z indicate the lateral and horizontal wake deflection, respectively, and depend on the downstream position x. C_T indicates the thrust coefficient, whereas $\sigma_{0,y}$ and $\sigma_{z,0}$ represent the initial wake widths at the turbine location. A feature of this model consists of assigning multiple wake expansion coefficients k_i at different downstream positions defined by the breakpoints b_i. The transition between different k_i values is smoothed using the function l.

The wake-induced mixing factor M is modeled as

$$M_j = \sum_{i \in T^{up}(j)} \frac{A_{ij}a_i}{\frac{x_j - x_i}{D}} + \frac{\beta^p}{d} \quad , \tag{A4}$$

dependent on the induction factor a, the area overlap A between turbine wakes and their relative downstream distances normalized with the rotor diameter D, but also by the helix amplitude β and the tunable coefficients p and d. Yaw-added mixing is neglected in this study.

Lastly, the wake deflection caused by the yaw misalignment γ is modeled as

$$\delta_y = \frac{k_{\text{def}} \cdot C_T \cdot \gamma}{1 + w_d \cdot M_j} \ln\left(\frac{\frac{x}{D} - c}{\frac{x}{D} + c}\right) \quad , \tag{A5}$$

with k_{def}, w_d, and c indicating tunable coefficients.

A2 Tuning of the turbine and wake models

This section describes the tuning process adopted to determine the values of the several coefficients mentioned in the description of the turbine and wake models.

https://doi.org/10.5194/wes-2025-265
Preprint. Discussion started: 8 December 2025

eawe european academy of wind energy
Open Access WIND ENERGY SCIENCE DISCUSSIONS

Table A1. LES settings adopted for the tuning process.

Domain settings	
Domain size	$L_x \times L_y \times L_z = 4.48 \times 4.48 \times 1.28\,\mathrm{km}^3$
Cell size (base)	$\Delta x \times \Delta y \times \Delta z = 10 \times 10 \times 10\,\mathrm{m}^3$
Cell size (refined)	$\Delta x_r \times \Delta y_r \times \Delta z_r = 5 \times 5 \times 5\,\mathrm{m}^3$
Refinement size	$L_{x,r} \times L_{y,r} \times L_{z,r} = 2.8 \times 1.12 \times 0.6\,\mathrm{km}^3$
Precursor settings	
Infow wind speed	U_∞ = 10 m s^{-1}
Infow wind direction	$\phi = 240^\circ$ (south-west)
Simulation length	$t_{LES} = 36000\,\mathrm{s}$
Time step	$\Delta t = 0.5\,\mathrm{s}$
Surface roughness	$z_0 = 0.001$
Turbulence intensity	I = 3–6%
Shear coefficient	$\alpha = 0.1$
Wind veer	$\phi = 5^\circ$
Inversion height	$z_i = 700\,\mathrm{m}$
Inversion strength	$\Delta\theta = 2.5\,\mathrm{K}$
Inversion thickness	$\Delta h = 100\,\mathrm{m}$
Lapse rate	$\Gamma = 1\,\mathrm{K\,km}^{-1}$
Wind turbine simulations	
Simulation length	$t_{LES} = 4200\,\mathrm{s}$
Time step LES	$\Delta t_{LES} = 0.05\,\mathrm{s}$
Time step OpenFAST	$\Delta t_{OF} = 0.01\,\mathrm{s}$
Turbine diameter	$D = 283\,\mathrm{m}$
Blade epsilon	$\epsilon = 2\Delta x_r = 10\,\mathrm{m}$
Rotor approximation	Actuator Line Method
Turbine spacing	$d = 4.5\,D$

The tuning procedure is based on a dataset obtained through multiple simulations performed with the LES solver AMR-Wind (Kuhn et al., 2025), which has been coupled with the aeroelastic simulator OpenFAST (National Renewable Energy Laboratory, 2024b) to model a wind turbine's response. The simulations were run with a conventionally neutral boundary layer at turbulence levels similar to those found at the North Sea. Multiple cases were simulated, covering different control strategies and layouts. An overview of the LES settings and the simulation cases are provided in Tables A1 and A2.

The tuning process has been decomposed into six sequential steps to improve its efficiency. Each of them involved a specific component of the wind farm model and a limited number of coefficients. These tuning phases have been executed in the following order:

https://doi.org/10.5194/wes-2025-265
Preprint. Discussion started: 8 December 2025

eawe european academy of wind energy
Open Access WIND ENERGY SCIENCE DISCUSSIONS

Table A2. LES cases adopted for the tuning process, specifying the number of turbines (N_{WT}), control settings (γ, β), and whether they were used for tuning the turbine or the wake model.

Simulation case	N_{WT}	**Control settings**	**Tuning purpose**
Loss coefficients	1	$\beta = \{0^\circ : 0.5^\circ : 5.5^\circ\}$	Turbine model
Baseline	1	$\gamma = 0^\circ$, $\beta = 0^\circ$	Wake model
Helix A2	1	$\gamma = 0^\circ$, $\beta = 2^\circ$	Wake model
Helix A3	1	$\gamma = 0^\circ$, $\beta = 3^\circ$	Wake model
Helix A4	1	$\gamma = 0^\circ$, $\beta = 4^\circ$	Wake model
Wake steering (+)	1	$\gamma = 20^\circ$, $\beta = 0^\circ$	Wake model
Wake steering (-)	1	$\gamma = -20^\circ$, $\beta = 0^\circ$	Wake model
Baseline array	3	$\gamma_i = [0^\circ, 0^\circ, 0^\circ]$, $\beta_i = [0^\circ, 0^\circ, 0^\circ]$	Wake model
Helix array A3	3	$\gamma_i = [0^\circ, 0^\circ, 0^\circ]$, $\beta_i = [3^\circ, 0^\circ, 0^\circ]$	Wake model
Helix array A4	3	$\gamma_i = [0^\circ, 0^\circ, 0^\circ]$, $\beta_i = [4^\circ, 0^\circ, 0^\circ]$	Wake model
Wake steering array	3	$\gamma_i = [15^\circ, 18^\circ, 0^\circ]$, $\beta_i = [0^\circ, 0^\circ, 0^\circ]$	Wake model

1. Turbine model (a, b_P, c_P, b_T, c_T)
2. Wake deficit model: one turbine ($\sigma_{0,D}, k_1, k_2$)
3. Wake deficit model: multiple turbines (w_v)
4. Wake deficit model: active wake mixing (p, d)
5. Wake deflection model: one turbine (k_{def}, c)
6. Wake deflection model: multiple turbines (w_d)

The results of the tuning process, i.e. the obtained values of the coefficients introduced by these models, are summarized in Table A3.

The turbine model is tuned by fitting the thrust and power loss ratios, defined as $C_T/C_{T,BL}$ and P/P_{BL}, respectively, to the corresponding data for different values of β, using the scipy function curve_fit. The results of this tuning phase are included in Fig. A1. The well established decreasing trend is observed as the amplitude increases, in alignment with the data obtained from OpenFAST/LES. In these plots, the curve obtained using the default coefficients available in FLORIS is also included, highlighting the importance of repeating the tuning process of these models for the specific case study.

For the tuning of the wake deficit and deflection models, the horizontal velocity profiles at hub height and multiple downstream distances are considered. Specifically, the scipy function least_squares is used to minimize the residuals between the cube values of the velocities, as a proxy of the power. Figures A2 and A3 describe the fit of the wake model with the LES data. Whereas Fig. A2 refers to the wake of only one turbine, Fig. A3 demonstrates the ability of the model to estimate the

https://doi.org/10.5194/wes-2025-265
Preprint. Discussion started: 8 December 2025

eawe european academy of wind energy
Open Access WIND ENERGY SCIENCE DISCUSSIONS

Table A3. Tuning coefficients of turbine and wake models.

Name	Symbol	Value	Unit
Helix amplitude exponent	a	1.907	$[-]$
Helix b coefficient (power)	b_P	$1.376 \cdot 10^{-3}$	$[-]$
Helix c coefficient (power)	c_P	$4.02 \cdot 10^{-11}$	$[\mathrm{kW}^{-1}]$
Helix b coefficient (thrust)	b_T	$8.371 \cdot 10^{-4}$	$[-]$
Helix c coefficient (thrust)	c_T	$5.084 \cdot 10^{-4}$	$[-]$
Initial wake width	$\sigma_{0,D}$	0.3042	$[\mathrm{m}]$
Wake expansion coeff. ($x \leq 10\,D$)	k_1	0.01213	$[-]$
Wake expansion coeff. ($x > 10\,D$)	k_2	0.008	$[-]$
Mixing gain velocity	w_v	0.2119	$[-]$
Active wake control exponent	p	1.119	$[-]$
Active wake control denominator	d	137.2	$[-]$
Deflection gain	k_{def}	2.098	$[\mathrm{m\,deg}^{-1}]$
Deflection rate	c	12.02	$[-]$
Mixing gain deflection	w_d	0.0	$[-]$

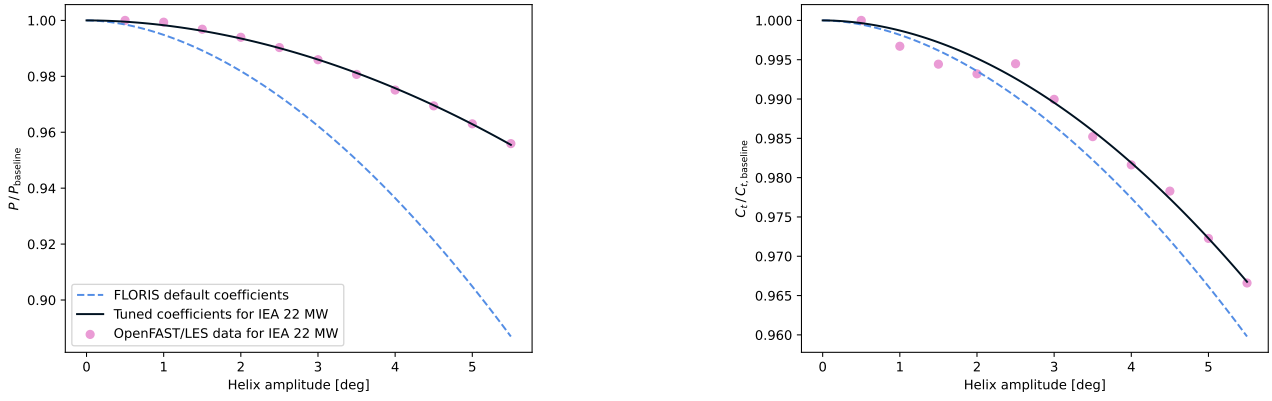

(a) Power loss comparison.

(b) Thrust loss comparison.

Figure A1. Comparison between the tuned turbine model and the OpenFAST/LES data for both (a) power loss and (b) thrust loss for different helix amplitudes. The functions obtained with the default coefficients available in FLORIS are also included.

wake caused by multiple turbines. In both cases, different operation modes are shown, including baseline, wake steering, and helix control. Whereas the wake characteristics of a single turbine can be fairly replicated by the model, in case of multiple turbines the error with the higher-fidelity data increases. Overall, the main trends can be captured by the engineering wake model, enabling a realistic estimation of the effect caused by the control strategy.

https://doi.org/10.5194/wes-2025-265
Preprint. Discussion started: 8 December 2025

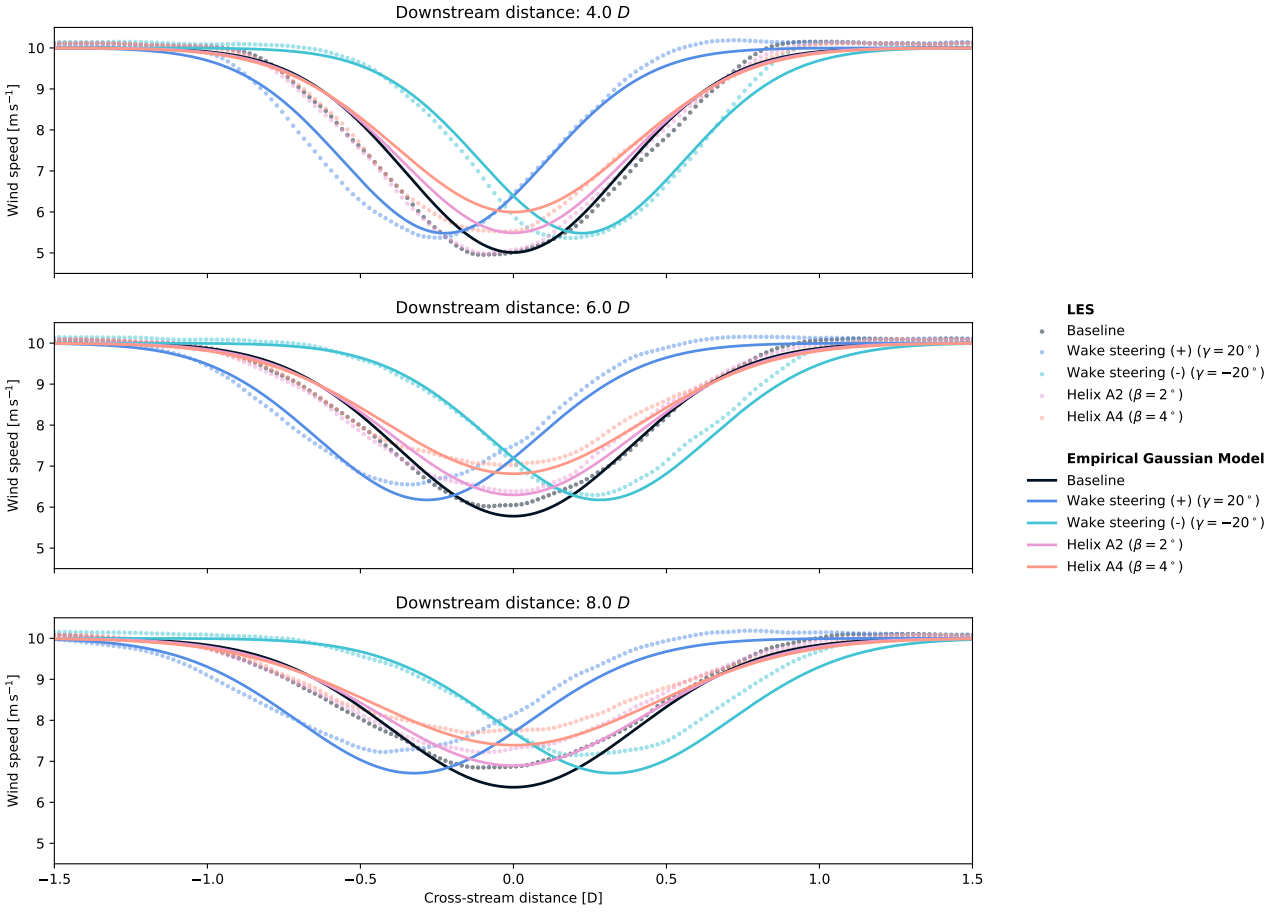

Figure A2. Wind speed deficit modeled using the Empirical Gaussian model and LES data, considering no control ("baseline"), wake steering and helix control, shown for down-stream distances of $4\,D$, $6\,D$, and $8\,D$. The plots refer to one-turbine simulations.

https://doi.org/10.5194/wes-2025-265
Preprint. Discussion started: 8 December 2025

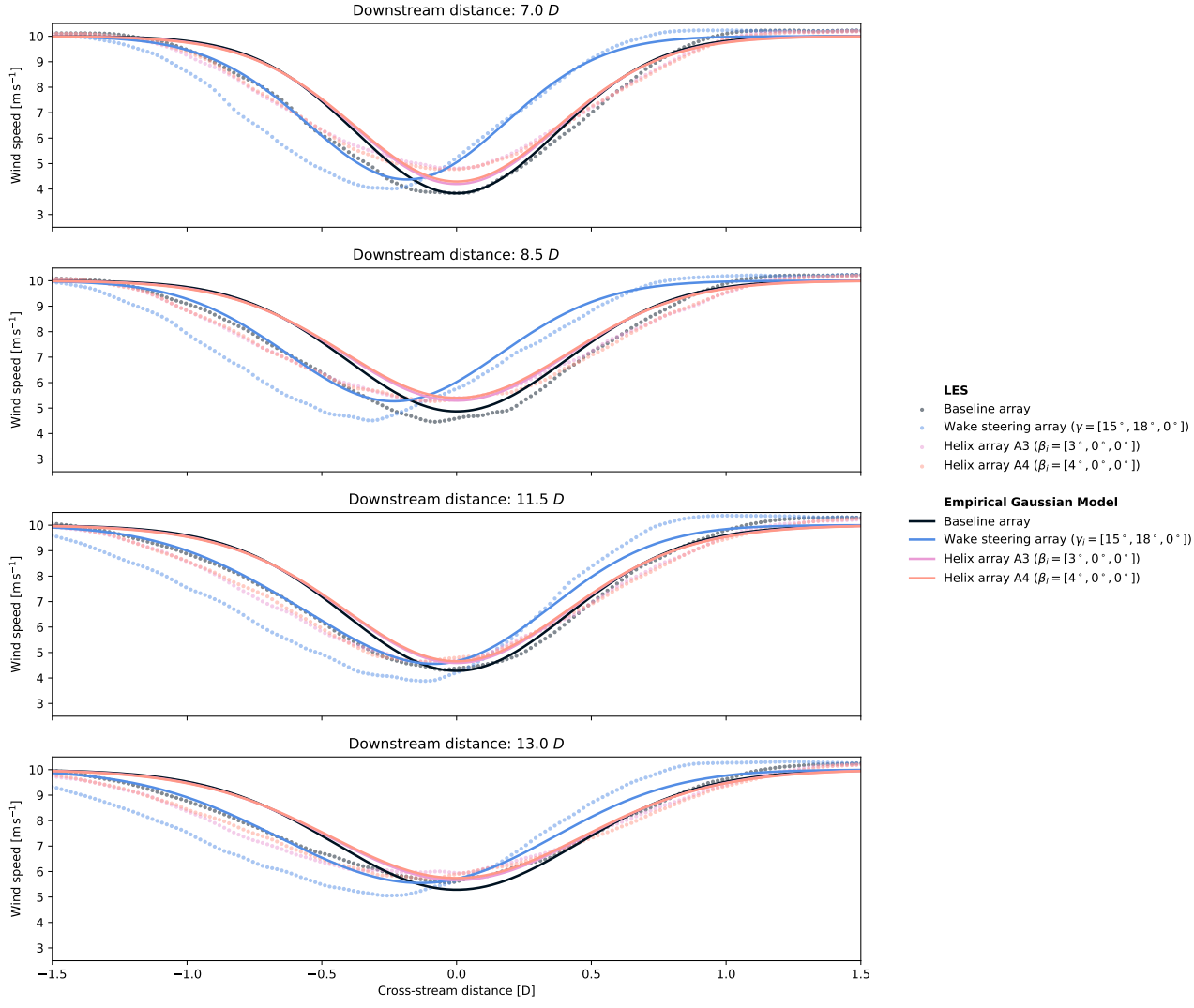

Figure A3. Wind speed deficit modeled using the Empirical Gaussian model and LES data, considering no control ("baseline"), wake steering and helix control, shown for down-stream distances of $7\,D$, $8.5\,D$, and $11.5\,D$. The plots refer to the simulations of three aligned turbines simulations, with a spacing of $4.5\,D$.

https://doi.org/10.5194/wes-2025-265
Preprint. Discussion started: 8 December 2025

eawe european academy of wind energy
Open Access WIND ENERGY SCIENCE DISCUSSIONS

Appendix B: Description of the Multi-strategy Serial-Refine (MSR) optimization algorithm

This appendix gives a comprehensive description of the optimization algorithm named Multi-strategy Serial-Refine (MSR) developed during this study. As mentioned in Sect. 2, the MSR has been designed to optimize multiple control strategies within a wind farm, aiming to maximize a generic objective function. The structure of the MSR is described in Fig. B1, where different blocks are highlighted.

First, an objective function f to maximize is defined. This is treated by the MSR as a black-box function that depends on the control variables contained in the two-dimensional control matrix $\mathbf{C}$, where the dimensions represent the different turbines and control strategies, respectively. The black-box nature of this function ensures that the algorithm remains entirely independent of specific solvers such as PyWake or FLORIS, thereby providing the user with a high degree of flexibility. Moreover, multiple objectives can be combined within this function, as implemented in this study. Overall, the goal of the algorithm is to find the optimal control matrix, denoted by $\mathbf{C}_{\mathrm{opt}}$, which provides the objective function value f_{opt}.

As mentioned in Sect. 2, the N_{wt} wind turbines are sorted in downstream order based on the wind direction and the algorithm iterates over each turbine N_{step} times. These iterations are indicated by the for loops included in Fig. B1. Compared to SR, where only the yaw angles are optimized at each turbine iteration, in the MSR the N different control strategies are optimized through parallel separated optimization blocks. The outputs of these modules are then processed by a coordination block after each turbine iteration, and by a refinement block after the termination of each step.

Algorithm B1 describes an example of an optimization block for turbine i and strategy j, which produces as output a temporary objective function value $f_{\mathrm{opt},j}$ and a temporary optimal control matrix $\mathbf{C}_{\mathrm{opt},j}$. Moreover, this block updates the ij-th element of the selected control matrix $\mathbf{C}_{\mathrm{sel}}$, which is the matrix that stores the optimal control values for all turbines and strategies neglecting any constraints of exclusivity between the strategies. First, the value of the objective function f_{opt}

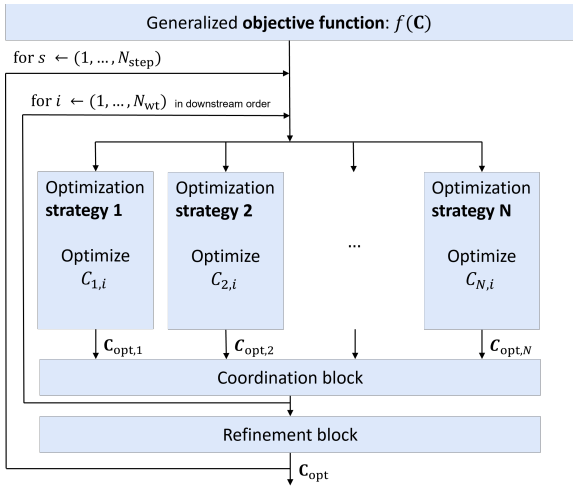

Figure B1. Structure of the Multi-strategy Serial-Refine (MSR) optimization algorithm.

https://doi.org/10.5194/wes-2025-265
Preprint. Discussion started: 8 December 2025

eawe european academy of wind energy
Open Access WIND ENERGY SCIENCE DISCUSSIONS

obtained from the previous iteration is copied into a temporary copy $f_{\mathrm{opt},j}$. Second, the control values $\boldsymbol{C}_{\mathrm{values,test}}$ of the strategy j that will be tested in this iteration are calculated. The vector $\boldsymbol{C}_{\mathrm{values,test}}$ is computed by adding the offset values $\boldsymbol{C}_{\mathrm{offset},j}$ obtained from the refinement block to the selected control value of strategy j obtained in the previous iteration for turbine i, i.e. the ij-th term of $\mathbf{C}_{\mathrm{sel}}$. The values of $\boldsymbol{C}_{\mathrm{values,test}}$ are then constrained by enforcing the lower and upper bounds $[c_{\mathrm{min},j}, c_{\mathrm{max},j}]$ provided by the user. Analogous to the SR, the values contained in $\boldsymbol{C}_{\mathrm{values,test}}$ are used to update the ij-th term of the control matrix $\mathbf{C}_{\mathrm{opt}}$, obtaining a new control matrix $\mathbf{C}_{\mathrm{test}}$. In case the strategy j is appointed as exclusive, the control values of any other strategy contained in the i-th row of $\mathbf{C}_{\mathrm{test}}$ are set to 0. This step has been expressed through the Kronecker delta in Algorithm B1. Then, the objective function value f_{test} is calculated based on $\mathbf{C}_{\mathrm{test}}$ and if it guarantees better performance, the algorithm updates $\mathbf{C}_{\mathrm{opt},j}$, $f_{\mathrm{opt},j}$, and the ij-th element of $\mathbf{C}_{\mathrm{sel}}$

Repeating this procedure for all the different control strategies, N temporary objective function values $f_{\mathrm{opt},j}$ and optimal control matrices $\mathbf{C}_{\mathrm{opt},j}$ are obtained. These are processed by the coordination block, which selects the best-performing $\mathbf{C}_{\mathrm{opt},j}$ by comparing the $f_{\mathrm{opt},j}$ values and then updates f_{opt} and $\mathbf{C}_{\mathrm{opt}}$ accordingly. Lastly, the refinement block updates the offset values $\boldsymbol{C}_{\mathrm{offset},j}$ for each strategy. Specifically, after each step, the search space of the optimal control variables is restricted around the temporary values found in the previous iteration. This is achieved by decreasing the range of the offsets that determine the value adopted for each turbine, similar to the traditional implementation of the SR.

A key feature of the algorithm is the use of the selected control matrix $\mathbf{C}_{\mathrm{sel}}$, rather than $\mathbf{C}_{\mathrm{opt}}$, i.e. the output of the coordination block. This choice improves the optimization process by retaining temporary optimal control values, preventing them from being lost when control strategies are exclusive. Specifically, when strategies are exclusive, all elements of the i-th row of $\mathbf{C}_{\mathrm{opt}}$ are zeros except for the element corresponding to the best-performing strategy at that iteration. Therefore, if the refinement stage were based directly on $\mathbf{C}_{\mathrm{opt}}$, the $\boldsymbol{C}_{\mathrm{values},j}$ of the other strategies would remain clustered around zero during the next steps. This would make the first iteration extremely influential. By instead relying on the selected control values of each strategy during the refinement, the algorithm is able to explore the design space more thoroughly, especially when two local optima correspond to different strategies, without prematurely converging to the strategy that guaranteed the best performance in the first iteration.

An example is depicted in Fig B2 to facilitate the comprehension of the MSR algorithm. The example refers to a wind farm consisting of three turbines, for which the MSR algorithm is used to optimize the WFFC operation when the wind direction is set to $270°$, i.e. wind coming from the left of the plot. Wake steering and the helix are the control strategies considered in this example, namely $N = 2$, and they are considered to be exclusive. The number of steps N_{step} and N_{values} are set to 2 and 3, respectively. The bounds for the yaw angles are $[-30°, 30°]$ while the helix amplitude is limited in the range $[0°, 5°]$.

The algorithm sorts the turbines in downstream order, thus identifying turbines 1, 2, and 3, as shown in the figure. Then, the algorithm iterates over turbine 1, testing 3 values of yaw angles, namely $[-30°, 0°, 30°]$. The bounds $[-30°, 30°]$ are enforced, but in this case no modification is required. The value $30°$ yields the best performance, hence it is assigned to the selected control matrix $\mathbf{C}_{\mathrm{sel}}$. Similarly, the values $[0°, 2.5°, 5°]$ are tested for the helix. After checking that the bounds are satisfied, the value $5°$ is selected as the best-performing, thus assigned to $\mathbf{C}_{\mathrm{sel}}$. The selected yaw angles and helix amplitude are indicated in the figure by the underline. Since the two strategies are exclusive, either wake steering or the helix can be applied to turbine 1.

https://doi.org/10.5194/wes-2025-265
Preprint. Discussion started: 8 December 2025

eawe european academy of wind energy
Open Access WIND ENERGY SCIENCE DISCUSSIONS

Algorithm B1 MSR: Optimization of the strategy j and the turbine i.

$f_{\text{opt},j} \leftarrow f_{\text{opt}}$
$\boldsymbol{C}_{\text{values,test}} \leftarrow \mathbf{C}_{\text{sel}}[i,j] + \boldsymbol{C}_{\text{offset},j}$
$\boldsymbol{C}_{\text{values,test}} \leftarrow \boldsymbol{C}_{\text{values,test}}$ constrained to $[c_{\min,j}, c_{\max,j}]$
for $c_{\text{value}} \leftarrow \boldsymbol{C}_{\text{values,test}}$ **do**
  $\mathbf{C}_{\text{test}} \leftarrow \mathbf{C}_{\text{opt}}$
  $\mathbf{C}_{\text{test}}[i,j] \leftarrow c_{\text{value}}$
  if strategy j is exclusive **then**
    for $j' \leftarrow 1$ to N **do**
      $\mathbf{C}_{\text{test}}[i,j'] \leftarrow \mathbf{C}_{\text{test}}[i,j'] \cdot \delta_{jj'}$
    end for
  end if
  $f_{\text{test}} \leftarrow f(\mathbf{C}_{\text{test}})$
  if $f_{\text{test}} > f_{\text{opt},j}$ **then**
    $f_{\text{opt},j} \leftarrow f_{\text{test}}$
    $\mathbf{C}_{\text{opt},j} \leftarrow \mathbf{C}_{\text{test}}$
    $\mathbf{C}_{\text{sel}}[i,j] \leftarrow c_{\text{value}}$
  end if
end for

The objective function values obtained from the best-performing control variables, i.e. yaw angle of $30°$ and helix amplitude of $5°$, are compared. In this case, the yaw angle of $30°$ outperforms the helix with an amplitude of $5°$, as indicated by the arrow in the figure. Therefore, the optimal control matrix $\mathbf{C}_{\text{opt}}$ is updated by setting the yaw angle to $30°$ and the helix amplitude to $0°$. Then, the algorithm proceeds to turbines 2 applying the same procedure. In this case, the same values of optimal yaw angle and helix amplitude are found, thus $\mathbf{C}_{\text{sel}}$ and $\mathbf{C}_{\text{opt}}$ are updated accordingly. Lastly, the first step of the algorithm is completed by applying the same procedure to turbine 3, yielding optimal values of $0°$ for both yaw angle and helix amplitude.

The second step starts by refining the control values of turbine 1. Specifically, the values $[15°, 30°, 30°]$ and $[3.75°, 5°, 5°]$ are tested for the yaw angle and the helix amplitude, respectively. These are obtained by applying an offset to the values contained in $\mathbf{C}_{\text{sel}}$ for turbine 1, and by enforcing the corresponding bounds of each strategy. This last operation causes some values to be repeated. In this case, a yaw angle of $15°$ and a helix amplitude of $3.75°$ are selected, with the latter outperforming the former. Therefore, the first rows of $\mathbf{C}_{\text{sel}}$ and $\mathbf{C}_{\text{opt}}$ are set to $[15°\ \ 3.75°]$ and $[0°\ \ 3.75°]$, respectively. Then, the same procedure is applied to turbine 2. The same values of control variables are selected, setting also the second row of $\mathbf{C}_{\text{sel}}$ to $[15°\ \ 3.75°]$. However, the objective function value is higher when a yaw angle of $15°$ is applied to turbine 2 than a helix amplitude of $3.75°$, thus the second row of $\mathbf{C}_{\text{opt}}$ is set to $[15°\ \ 0°]$. Lastly, the algorithm iterates over turbine 3, whose selected and optimal control values are all equal to $0°$ for both strategies. Therefore, the optimal control strategy yielded by the MSR algorithm in this example consists of:

https://doi.org/10.5194/wes-2025-265
Preprint. Discussion started: 8 December 2025

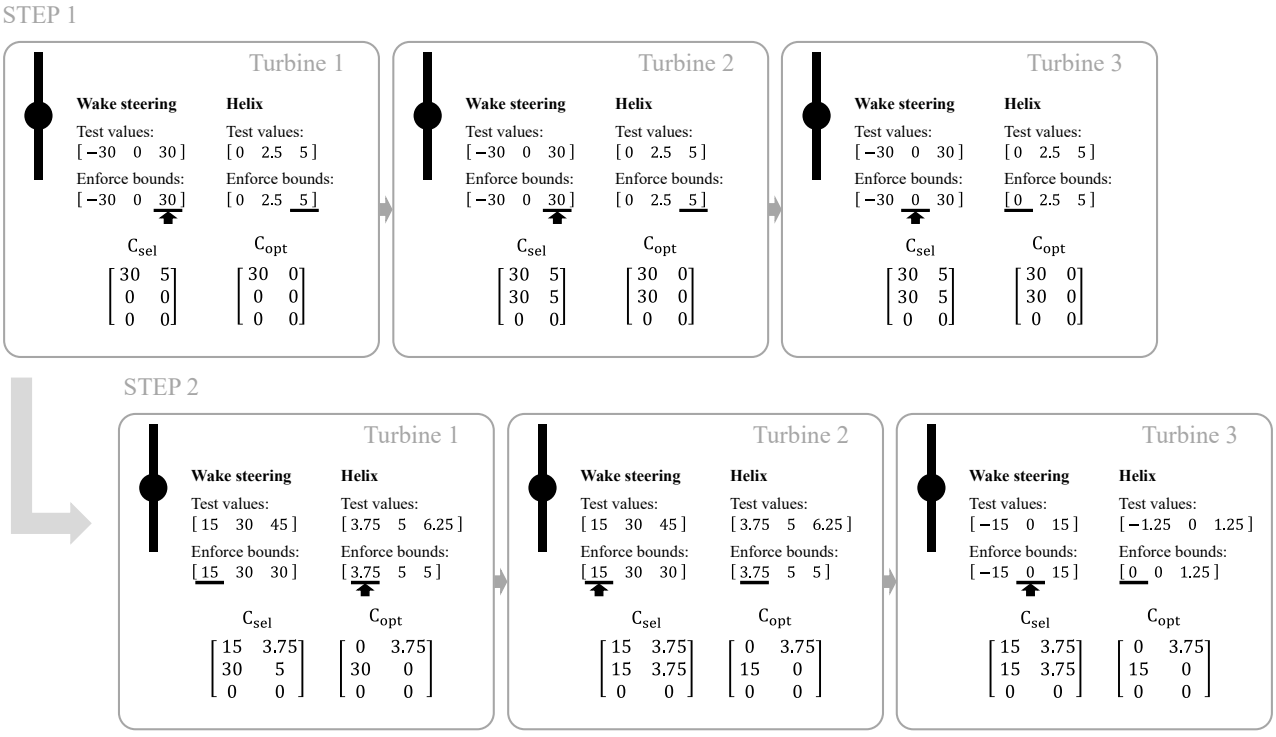

Figure B2. Example of the MSR working principle for three turbines with a wind direction of $270°$, i.e. wind coming from the left of the figure. At each step and turbine, the underline indicates the selected control value for every strategy while the arrow shows the best-performing control value among different strategies.

- Turbine 1 operating the helix with an amplitude of $3.75°$
- Turbine 2 applying wake steering with a yaw angle of $15°$
- Turbine 3 executes none of the two strategies

This example highlights the importance of using $\mathbf{C}_{\text{sel}}$ instead of $\mathbf{C}_{\text{opt}}$ to calculate the values of the control variables tested at each iteration. In the first step, the optimal control variables obtained for turbine 1 are a yaw angle of $30°$ and a helix amplitude of $0°$, due to the better performance of wake steering with respect to the helix for the tested values. In the second step, the situation for turbine 1 is reversed: the helix with an amplitude of $3.75°$ outperforms wake steering for the tested values. However, in case the values of $\mathbf{C}_{\text{opt}}$ obtained after the first step were used to refine the helix amplitudes tested in the second step, that would have resulted in testing $[-1.25°, 0°, 1.25°]$. Therefore, the optimal helix amplitude value of $3.75°$ would not have been tested, thus probably obtaining the yaw angle of $15°$ as the final decision for turbine 1, leading to a sub-optimal solution.

https://doi.org/10.5194/wes-2025-265
Preprint. Discussion started: 8 December 2025

eawe european academy of wind energy
Open Access WIND ENERGY SCIENCE DISCUSSIONS

Author contributions. Matteo Baricchio: conceptualisation, methodology, software, validation, investigation, writing – original draft, visualisation. Daan van der Hoek: writing – review & editing, methodology, software, validation. Tim Dammann: writing – review & editing, software, validation. Pieter M.O. Gebraad: writing – review & editing, conceptualisation, supervision. Jenna Iori: writing – review & editing, conceptualisation, supervision. Jan-Willem van Wingerden: writing – review & editing, conceptualisation, supervision, resources, funding acquisition.

Competing interests. At least one of the (co-)authors is an Associate editor of Wind Energy Science.

Financial support. This work has been supported by the SUDOCO project, which receives the funding from the European Union's Horizon Europe Programme under the grant No. 101122256.

https://doi.org/10.5194/wes-2025-265
Preprint. Discussion started: 8 December 2025

eawe european academy of wind energy
Open Access WIND ENERGY SCIENCE DISCUSSIONS

References

Anand, A., Braunbehrens, R., Guilloré, A., and Bottasso, C. L.: Economic lifetime-aware wind farm control, Wind Energy Science Discussions, 2025, 1–39, https://doi.org/10.5194/wes-2025-67, 2025.

Bechmann, A. and Quick, J.: Market-Driven Wind Resource Assessment, in: WindEurope Annual Event 2025, no. 1 in Journal of Physics: Conference Series, IOP Publishing, United Kingdom, https://doi.org/10.1088/1742-6596/3025/1/012001, windEurope Annual Event 2025, WindEurope ; Conference date: 08-04-2025 Through 10-04-2025, 2025.

Becker, M., Lejeune, M., Chatelain, P., Allaerts, D., Mudafort, R., and van Wingerden, J. W.: A dynamic open-source model to investigate wake dynamics in response to wind farm flow control strategies, Wind Energy Science, 10, 1055–1075, https://doi.org/10.5194/wes-10-1055-2025, 2025a.

Becker, M., van den Broek, M. J., Allaerts, D., and van Wingerden, J. W.: Closed-loop model-predictive wind farm flow control under time-varying inflow using FLORIDyn, https://arxiv.org/abs/2503.02790, 2025b.

Brown, K., Yalla, G., Cheung, L., Frederik, J., Houck, D., deVelder, N., Simley, E., and Fleming, P.: Comparison of wind-farm control strategies under realistic offshore wind conditions: wake quantities of interest, Wind Energy Science Discussions, 2025, 1–39, https://doi.org/10.5194/wes-2024-191, 2025.

Campagnolo, F., Weber, R., Schreiber, J., and Bottasso, C. L.: Wind tunnel testing of wake steering with dynamic wind direction changes, Wind Energy Science, 5, 1273–1295, https://doi.org/10.5194/wes-5-1273-2020, 2020.

Dammann, T., van der Hoek, D., Yu, W., and van Wingerden, J.-W.: Enhanced Wind Farm Performance via Active Wake Control: A Steady-State Approach, in: 2025 American Control Conference (ACC), pp. 2856–2861, https://doi.org/10.23919/ACC63710.2025.11107695, 2025.

Doekemeijer, B. M., Kern, S., Maturu, S., Kanev, S., Salbert, B., Schreiber, J., Campagnolo, F., Bottasso, C. L., Schuler, S., Wilts, F., Neumann, T., Potenza, G., Calabretta, F., Fioretti, F., and van Wingerden, J. W.: Field experiment for open-loop yaw-based wake steering at a commercial onshore wind farm in Italy, Wind Energy Science, 6, 159–176, https://doi.org/10.5194/wes-6-159-2021, 2021.

Fleming, P. A., Gebraad, P. M., Lee, S., van Wingerden, J. W., Johnson, K., Churchfield, M., Michalakes, J., Spalart, P., and Moriarty, P.: Evaluating techniques for redirecting turbine wakes using SOWFA, Renewable Energy, 70, 211–218, https://doi.org/https://doi.org/10.1016/j.renene.2014.02.015, special issue on aerodynamics of offshore wind energy systems and wakes, 2014.

Fleming, P. A., Stanley, A. P. J., Bay, C. J., King, J., Simley, E., Doekemeijer, B. M., and Mudafort, R.: Serial-Refine Method for Fast Wake-Steering Yaw Optimization, Journal of Physics: Conference Series, 2265, 032 109, https://doi.org/10.1088/1742-6596/2265/3/032109, 2022.

Frederik, J. A. and van Wingerden, J.-W.: On the load impact of dynamic wind farm wake mixing strategies, Renewable Energy, 194, 582–595, https://doi.org/https://doi.org/10.1016/j.renene.2022.05.110, 2022.

Frederik, J. A., Doekemeijer, B. M., Mulders, S. P., and van Wingerden, J. W.: The helix approach: Using dynamic individual pitch control to enhance wake mixing in wind farms, Wind Energy, 23, 1739–1751, https://doi.org/https://doi.org/10.1002/we.2513, 2020.

Frederik, J. A., Simley, E., Brown, K. A., Yalla, G. R., Cheung, L. C., and Fleming, P. A.: Comparison of wind farm control strategies under realistic offshore wind conditions: turbine quantities of interest, Wind Energy Science, 10, 755–777, https://doi.org/10.5194/wes-10-755-2025, 2025.

https://doi.org/10.5194/wes-2025-265
Preprint. Discussion started: 8 December 2025

Gebraad, P. M. O., Teeuwisse, F. W., van Wingerden, J. W., Fleming, P. A., Ruben, S. D., Marden, J. R., and Pao, L. Y.: Wind plant power optimization through yaw control using a parametric model for wake effects—a CFD simulation study, Wind Energy, 19, 95–114, https://doi.org/https://doi.org/10.1002/we.1822, 2016.

Gray, J. S., Hwang, J. T., Martins, J. R. R. A., Moore, K. T., and Naylor, B. A.: OpenMDAO: An open-source framework for multidisciplinary design, analysis, and optimization, Structural and Multidisciplinary Optimization, 59, 1075–1104, https://doi.org/10.1007/s00158-019-02211-z, 2019.

Guilloré, A., Campagnolo, F., and Bottasso, C. L.: A control-oriented load surrogate model based on sector-averaged inflow quantities: capturing damage for unwaked, waked, wake-steering and curtailed wind turbines, Journal of Physics: Conference Series, 2767, 032 019, https://doi.org/10.1088/1742-6596/2767/3/032019, 2024.

Hodgson, E. L. and Andersen, S. J.: Wake steering under inflow wind direction uncertainty: an LES study, Wind Energy Science Discussions, 2025, 1–26, https://doi.org/10.5194/wes-2025-243, 2025.

Jimenez, A., Crespo, A., and Migoya, E.: Application of a LES technique to characterize the wake deflection of a wind turbine in yaw, Wind Energy, 13, 559–572, https://doi.org/https://doi.org/10.1002/we.380, 2010.

Kainz, S., Scherzl, A., Guilloré, A., Anand, A., and Bottasso, C. L.: An initial study on the environmental value of wind farm control, Journal of Physics: Conference Series, 3131, 012 044, https://doi.org/10.1088/1742-6596/3131/1/012044, 2025.

Kuhn, M. B., Henry de Frahan, M. T., Mohan, P., Deskos, G., Churchfield, M., Cheung, L., Sharma, A., Almgren, A., Ananthan, S., Brazell, M. J., A., M. L., Thedin, R., Rood, J., Sakievich, P., Vijayakumar, G., Zhang, W., and Sprague, M. A.: AMR-Wind: A performance-portable, high-fidelity flow solver for wind farm simulations, Wind Energy, 28, –, https://doi.org/10.1002/we.70010, 2025.

Liew, J., Urbán, A. M., and Andersen, S. J.: Analytical model for the power–yaw sensitivity of wind turbines operating in full wake, Wind Energy Science, 5, 427–437, https://doi.org/10.5194/wes-5-427-2020, 2020.

Meyers, J., Bottasso, C., Dykes, K., Fleming, P., Gebraad, P., Giebel, G., Göçmen, T., and van Wingerden, J. W.: Wind farm flow control: prospects and challenges, Wind Energy Science, 7, 2271–2306, https://doi.org/10.5194/wes-7-2271-2022, 2022.

Mühle, F. V., Heckmeier, F. M., Campagnolo, F., and Breitsamter, C.: Wind tunnel investigations of an individual pitch control strategy for wind farm power optimization, Wind Energy Science, 9, 1251–1271, https://doi.org/10.5194/wes-9-1251-2024, 2024.

Munters, W. and Meyers, J.: Towards practical dynamic induction control of wind farms: analysis of optimally controlled wind-farm boundary layers and sinusoidal induction control of first-row turbines, Wind Energy Science, 3, 409–425, https://doi.org/10.5194/wes-3-409-2018, 2018.

National Renewable Energy Laboratory: FLORIS Version 4.4, https://github.com/NREL/floris, last accessed: 13 July 2025, 2024a.

National Renewable Energy Laboratory: OpenFAST: An Open-Source Wind Turbine Simulation Tool, https://github.com/OpenFAST/openfast, version 3.5.0, 2024b.

Pedersen, J. G., Svensson, E., Poulsen, L., and Nygaard, N. G.: Turbulence Optimized Park model with Gaussian wake profile, Journal of Physics: Conference Series, 2265, 022 063, https://doi.org/10.1088/1742-6596/2265/2/022063, 2022.

Pedersen, M. M., Forsting, A. M., van der Laan, P., Riva, R., Romàn, L. A. A., Risco, J. C., Friis-Møller, M., Quick, J., Christiansen, J. P. S., Rodrigues, R. V., Olsen, B. T., and Réthoré, P.-E.: PyWake 2.5.0: An open-source wind farm simulation tool, https://gitlab.windenergy.dtu.dk/TOPFARM/PyWake, 2023.

Quick, J., Annoni, J., King, R., Dykes, K., Fleming, P., and Ning, A.: Optimization Under Uncertainty for Wake Steering Strategies, Journal of Physics: Conference Series, 854, 012 036, https://doi.org/10.1088/1742-6596/854/1/012036, 2017.

https://doi.org/10.5194/wes-2025-265
Preprint. Discussion started: 8 December 2025

Quick, J., King, J., King, R. N., Hamlington, P. E., and Dykes, K.: Wake steering optimization under uncertainty, Wind Energy Science, 5, 413–426, https://doi.org/10.5194/wes-5-413-2020, 2020.

Rott, A., Doekemeijer, B., Seifert, J. K., van Wingerden, J. W., and Kühn, M.: Robust active wake control in consideration of wind direction variability and uncertainty, Wind Energy Science, 3, 869–882, https://doi.org/10.5194/wes-3-869-2018, 2018.

Simley, E., Fleming, P., and King, J.: Design and analysis of a wake steering controller with wind direction variability, Wind Energy Science, 5, 451–468, https://doi.org/10.5194/wes-5-451-2020, 2020.

Simley, E., Millstein, D., Jeong, S., and Fleming, P.: The value of wake steering wind farm flow control in US energy markets, Wind Energy Science, 9, 219–234, https://doi.org/10.5194/wes-9-219-2024, 2024.

Taschner, E., van Vondelen, A., Verzijlbergh, R., and van Wingerden, J. W.: On the performance of the helix wind farm control approach in the conventionally neutral atmospheric boundary layer, Journal of Physics: Conference Series, 2505, 012 006, https://doi.org/10.1088/1742-6596/2505/1/012006, 2023.

Taschner, E., Becker, M., Verzijlbergh, R., and Van Wingerden, J. W.: Comparison of helix and wake steering control for varying turbine spacing and wind direction, Journal of Physics: Conference Series, 2767, 032 023, https://doi.org/10.1088/1742-6596/2767/3/032023, 2024.

van Beek, M. T., Viré, A., and Andersen, S. J.: Sensitivity and Uncertainty of the FLORIS Model Applied on the Lillgrund Wind Farm, Energies, 14, https://doi.org/10.3390/en14051293, 2021.

van der Hoek, D., Doekemeijer, B., Andersson, L. E., and van Wingerden, J. W.: Predicting the benefit of wake steering on the annual energy production of a wind farm using large eddy simulations and Gaussian process regression, Journal of Physics: Conference Series, 1618, 022 024, https://doi.org/10.1088/1742-6596/1618/2/022024, 2020.

van der Hoek, D., den Abbeele, B. V., Simao Ferreira, C., and van Wingerden, J. W.: Maximizing wind farm power output with the helix approach: Experimental validation and wake analysis using tomographic particle image velocimetry, Wind Energy, 27, 463–482, https://doi.org/https://doi.org/10.1002/we.2896, 2024.

van Vondelen, A. A., Navalkar, S. T., Kerssemakers, D. R., and van Wingerden, J. W.: Enhanced wake mixing in wind farms using the Helix approach: A loads sensitivity study, in: 2023 American Control Conference (ACC), pp. 831–836, https://doi.org/10.23919/ACC55779.2023.10155965, 2023.

van Vondelen, A. A. W., Coquelet, M., Navalkar, S. T., and van Wingerden, J. W.: Synchronized Helix Wake Mixing Control, Wind Energy Science Discussions, 2025, 1–36, https://doi.org/10.5194/wes-2025-51, 2025.

van Wingerden, J. W., Fleming, P. A., Göçmen, T., Eguinoa, I., Doekemeijer, B. M., Dykes, K., Lawson, M., Simley, E., King, J., Astrain, D., Iribas, M., Bottasso, C. L., Meyers, J., Raach, S., Kölle, K., and Giebel, G.: Expert Elicitation on Wind Farm Control, Journal of Physics: Conference Series, 1618, 022 025, https://doi.org/10.1088/1742-6596/1618/2/022025, 2020.

Virtanen, P., Gommers, R., Oliphant, T. E., Haberland, M., Reddy, T., Cournapeau, D., Burovski, E., Peterson, P., Weckesser, W., Bright, J., van der Walt, S. J., Brett, M., Wilson, J., Millman, K. J., Mayorov, N., Nelson, A. R. J., Jones, E., Kern, R., Larson, E., Carey, C. J., Polat, İ., Feng, Y., Moore, E. W., VanderPlas, J., Laxalde, D., Perktold, J., Cimrman, R., Henriksen, I., Quintero, E. A., Harris, C. R., Archibald, A. M., Ribeiro, A. H., Pedregosa, F., van Mulbregt, P., and SciPy 1.0 Contributors: SciPy 1.0: Fundamental Algorithms for Scientific Computing in Python, Nature Methods, 17, 261–272, https://doi.org/10.1038/s41592-019-0686-2, 2020.

von Brandis, A., Centurelli, G., Schmidt, J., Vollmer, L., Djath, B., and Dörenkämper, M.: An investigation of spatial wind direction variability and its consideration in engineering models, Wind Energy Science, 8, 589–606, https://doi.org/10.5194/wes-8-589-2023, 2023.

Vortex FDC: Vortex Wind Map, Accessed via Youwind, https://youwindrenewables.com, accessed: 2024-11-01, 2024.

https://doi.org/10.5194/wes-2025-265
Preprint. Discussion started: 8 December 2025

Zahle, F., Barlas, T., Lønbæk, K., Bortolotti, P., Zalkind, D., Wang, L., Labuschagne, C., Sethuraman, L., and Barter, G.: Definition of the IEA Wind 22-Megawatt Offshore Reference Wind Turbine, Tech. Rep. DTU Wind Energy Report E-0243, Department of Wind and Energy Systems, Technical University of Denmark, Roskilde, Denmark, ISBN 978-87-87335-71-3, https://doi.org/10.11581/DTU.00000317, 2024.